Validation and application of bearing and block tearing resistance Background to prEN1993-1-8:2021

Može, Primož; Yang, Fei; Veljkovic, Milan

DOI
10.1016/j.jcsr.2021.106985

Publication date
2021

Document Version
Final published version

Published in
Journal of Constructional Steel Research

Citation (APA)
Može, P., Yang, F., & Veljkovic, M. (2021). Validation and application of bearing and block tearing resistance: Background to prEN1993-1-8:2021. *Journal of Constructional Steel Research*, *187*, Article 106985. https://doi.org/10.1016/j.jcsr.2021.106985

Journal of Constructional Steel Research 187 (2021) 106985

Contents lists available at ScienceDirect

Journal of Constructional Steel Research

journal homepage: www.elsevier.com/locate/jcsr

Validation and application of bearing and block tearing resistance; background to prEN1993-1-8:2021

Primož Može [a,*], Fei Yang [b,c], Milan Veljkovic [b]

[a] University of Ljubljana, Faculty of Civil and Geodetic Engineering, Slovenia
[b] Department of Engineering Structures, Delft University of Technology, Delft, the Netherlands
[c] Department of Bridge Engineering, Tongji University, Shanghai, China

ARTICLE INFO

Keywords:
Eurocode
Finite element analysis
Bolted connections
Bearing
Block tearing
Damage initiation

ABSTRACT

An investigation of bolted connections with a specific geometry and bolt arrangement that require high local ductility to achieve the predicted resistances according to the design rules of the new prEN 1993-1-8 is presented. The experimental campaign includes tensile and shear tests on mild steel coupons to calibrate the parameters used for the true stress-strain relationship, damage initiation criterion and fracture evolution, while a numerical model for the high strength steel grade S690 was selected from the literature. The FEA results were satisfactorily validated by experiments on bolted connections for which the rules of the new prEN 1993-1-8:2021 were used to predict the resistance and deformation behaviour. The deformation behaviour was predicted by applying the new analytical model to calculate the deformation at the bolt hole due to the bearing action. The resistances of the tested connections were also predicted using EN 1993-1-8:2005. It is clearly shown that the new design formulae predict the experimental results significantly better than the results obtained according to EN 1993-1-8:2005. The FEA of a bolt group in bending, representing a high web splice, provides new proof for an analytical model for the distribution of forces between the bolts in the elastic stage and at ultimate resistance. Furthermore, the new Eurocode approach for predicting the bearing deformation behaviour at the bolt hole agreed well with the experimental and numerical results.

1. Introduction

Structural Eurocodes which are regarded as one of the most technically advanced series of standards for structural design, were subjected to a systematic review since the end of 2014. TC250 is CEN's committee in charge of the successful delivery of the programme developed in response to the European Commission's Mandate M/515 for amending and extending the scope of existing structural Eurocodes. The main objectives of the revision are: (i) improvement the ease of use, (ii) a reduction in the number of national determined parameters (NDPs), (iii) assessment, reuse and retrofitting of existing structures and (iv) improving requirements for robustness. The drafting of the revised standards began end of 2015 and was done by project teams, where its members were selected on the international tenders. The Eurocode for design of joints in steel structures EN 1993-1-8 [1] was in the first group of the standards, together with EN 1993-1-1 [2], that underwent the revision. The revised prEN 1993-1-8 was in April 2020 accepted by subcommittee for design of steel structures CEN/TC 250/SC 3. The members of the working group CEN/TC 250/SC 3 WG8 were involved in creating of approximately 200 pages of prEN1993-1-8:2020 with the help of the national mirror groups. Before the final version is publicly available, the standard was edited and internally denoted prEN 1993-1-8:2021 [3] for CEN formal enquiry procedure which is expected to end by a final formal voting foreseen at the end of 2022.

The revised prEN 1993-1-8:2021 [3] updates categories of bolted connections. Bearing type bolted connections (Category A) use bolts from property class 4.6 up to and including property class 10.9 in normal round holes, or slotted holes, where the longitudinal axis of the slotted hole is perpendicular to the direction of the force. Neither preloading nor special provisions for contact surfaces are required. In the draft prEN 1993-1-8:2021, the design shear resistance of bolt remains unchanged, while new formulas for the design bearing resistance per bolt and the design block tearing resistance were adopted. The design bearing resistance assumes average bearing stress in the plate, which depends on the relative end distance e_1/d_0 or the spacing between the bolts p_1/d_0 in the direction of the bearing force, and it is independent of the distance

* Corresponding author.
E-mail address: primoz.moze@fgg.uni-lj.si (P. Može).

https://doi.org/10.1016/j.jcsr.2021.106985
Received 7 July 2021; Received in revised form 24 September 2021; Accepted 26 September 2021
Available online 8 October 2021

perpendicular to the bearing force.

$$F_{\mathrm{b,Rd}} = \frac{k_{\mathrm{m}} \alpha_{\mathrm{b}}\, d\, t f_{\mathrm{u}}}{\gamma_{\mathrm{M2}}} \tag{1}$$

$$\alpha_b = \begin{cases} min\left(\frac{e_1}{d_0};\ 3\frac{f_{\mathrm{ub}}}{f_u};3\right); \text{for end bolt} \\ min\left(\frac{p_1}{d_0} - \frac{1}{2};\ 3\frac{f_{\mathrm{ub}}}{f_{\mathrm{u}}};3\right); \text{for inner bolt} \end{cases} \tag{2}$$

where f_{u} is the nominal ultimate tensile strength of the steel plate, f_{ub} is the nominal ultimate tensile strength of the bolt, d_0 is the bolt hole diameter, d the bolt diameter and γ_{M2} is the partial factor with the recommended value of 1.25. The material parameter k_{m} is 1 except for steel grades equal to or greater than S460, for which k_{m} is 0.9. The coefficient α_{b} accounts for the end effects with the upper limit of 3, which ensures the development of the full bearing resistance at the remaining bolt holes in a connection considering that the distances e_2 and p_2 are sufficient to prevent fracture in the net area in tension. Otherwise, the design resistance is indirectly controlled by the design for block tearing or the net cross-section resistance. Although this statement was justified by the statistical evaluation of 1264 experimental results in [4], one of the objectives of this paper is to show whether structural steels (S355 to S690) have sufficient ductility to develop high bearing resistance also for very specific connection geometries. However, a reduction of bearing resistance should be considered for specific cases, where bolt row is positioned close to the plate edge should be considered as in case of an angle connected by one bolt. The bearing resistance should not exceed:

$$N_{\mathrm{u,Rd}} = \frac{2(e_2 - d_0/2)\, t f_{\mathrm{u}}}{\gamma_{\mathrm{M2}}} \tag{3}$$

where e_2 is the edge distance (the distance from the bolt hole centre to the plate edge parallel to the bearing force). Eq. (3) was shown to be conservative even in case of angles connected by one bolt, where the moment due to the force eccentricity is present and can be neglected [4]. Therefore, the main motivation of this reduction is to discourage a designer from designing connections with the combination of small edge distance e_2 and large bolt spacing p_1 and large end distance e_1. Fig. 1 shows the effect of the reduction of the bearing resistance. The vertical axis shows minimum of the ratio $N_{\mathrm{u,Rd}}/F_{\mathrm{b,Rd}}$ and 1, where $N_{\mathrm{u,Rd}}$ and $F_{\mathrm{b,Rd}}$ are obtained by Eq. (1) and Eq. (3). The reduction of the bearing resistance has no effect if the factor α_{b} is equal to or smaller than 1.5 ($e_1 \leq 1.5d_0$). For the maximum value of $\alpha_{\mathrm{b}} = 3$, about 50% reduction is observed for the edge distance $e_2 = 1.2d_0$, while no reduction is necessary when the edge distance e_2 exceeds $1.86d_0$.

The bearing resistance as presented in EN 1993-1-8:2005 [1] prevents shear failure associated with a shorter end distance or bolt spacing. The upper limit of average bearing stress of $2.5f_u$ that develops at large distances controls the hole elongation. EN 1993-1-8 defines the design bearing resistance per bolt as:

$$F_{b,Rd} = \frac{k_1 \alpha_b f_u dt}{\gamma_{M2}} \tag{4}$$

where the partial factor γ_{M2} has the recommended value of 1.25. The parameters α_b and k_1 are defined as follows, taking mainly geometrical parameters into account:

- in the direction of load transfer

$$\alpha_b = min\left(\alpha_d; \frac{f_{ub}}{f_u};\ 1\right) \tag{5}$$

$$\alpha_d = \frac{e_1}{3d_0}, \text{for end bolts} \tag{6}$$

$$\alpha_d = \frac{p_1}{3d_0} - \frac{1}{4}, \text{for inner bolts} \tag{7}$$

- perpendicular to the direction of load transfer

$$k_1 = min\left(2.8\frac{e_2}{d_0} - 1.7; 1.4\frac{p_2}{d_0} - 1.7; 2.5\right), \text{for edge bolts} \tag{8}$$

$$k_1 = min\left(1.4\frac{p_2}{d_0} - 1.7; 2.5\right), \text{for inner bolts} \tag{9}$$

The design bearing resistance of group of bolts governs the design when the distances perpendicular to the bearing force are large enough to prevent fracture in the net area in tension. It can be obtained by the summation of individual bearing resistances when the ductility is assured. This occures when the design shear resistance of each individual bolt is greater than or equal to its design bearing resistance. Otherwise, the design bearing resistance of group of bolts is taken as the number of bolts multiplied by the smallest design resistance of any individual bolt. For long connections, the unequal distribution of the bearing forces among bolts is considered by the reduction of the design shear resistance of bolts.

The design block tearing resistance, which is based on the AISC [5] block tearing strength function, governs the design when the distances perpendicular to the bearing force are small enough that the interaction of bearing forces leads to the failure of the area surrounding the bolt group:

$$V_{eff,1,Rd} = \frac{A_{nt} f_u + min\left(A_{nv} f_u; A_{gv} f_y\right)/\sqrt{3}}{\gamma_{\mathrm{M2}}} \tag{10}$$

where A_{nt} is net area subjected to tension, A_{gv} is the gross area subjected to shear, A_{nv} is net area subjected to shear and f_{y} is the yield stress. For a

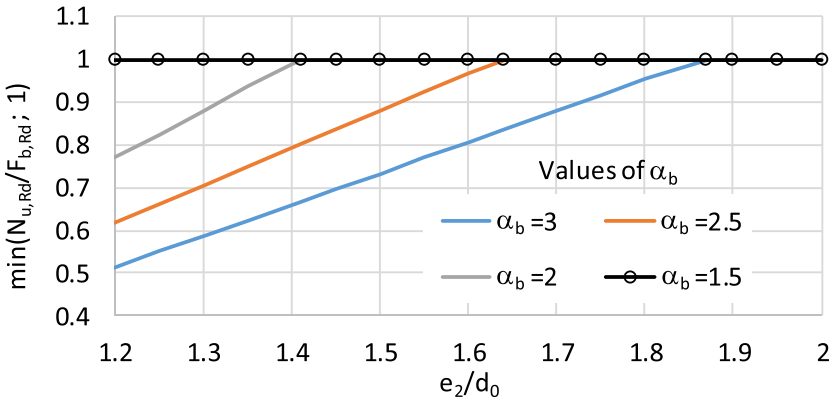

Fig. 1. Effects of the proposed reduction on the bearing resistance for bolts M20, $d_0 = 22$ mm.

bolt group where the tension stress acting on the tension area is non-uniform, the stress in the net area subjected to tension should be multiplied by 0.5. EN 1993-1-8:2005 [1] provides more conservative formulation for the block tearing where the net area subjected to shear is stressed to yield stress in pure shear $f_y/\sqrt{3}$.

Draft prEN 1993-1-8:2021 [3] provides an alternative method for calculation of the bearing deformation at bolt holes. The new formulation considers the nonlinearity, which is related to the embedding of the bolt, which causes a local yielding at the edge of the bolt hole. Therefore, it does not depend on the distances of the bolt hole from the plate edges. The embedding of the bolt can be described as follows:

$$\overline{\sigma}_b = \frac{126u/d}{\left(1+\sqrt{30u/d}\right)^2} \tag{11}$$

where $\overline{\sigma}_b$ is the normalized bearing stress, u/d is the normalized bolt hole deformation (see Fig. 2). A normalized nonlinear bearing deformation behaviour was originally proposed by Richard and Elsalti [6] and was adapted by Rex and Easterling [7]. Može [8,9] further simplified the bearing deformation model to appropriately consider the bolt embedding, plastic behaviour and steel grade. The embedding, which presents the validity of Eq. (11), is carried out up to 80% of the maximum bearing resistance for grades up to S460 and up to full bearing resistance for S460 and higher grades, as shown in Fig. 3. Plastic behaviour may be assumed from that point onwards, where the material in front of the bolts is fully yielded and allows large deformations with linearly increasing resistance up to the maximum bearing resistance. The bolt hole deformation at the maximum bearing resistance was obtained from the experimental results [10] and can be predicted by following equations, not included in prEN 1993-1-8 [3]:

$$u_{Xd} = min\left(\frac{k_m\alpha_b}{3}; k_m^2\right)\cdot d \tag{12}$$

where k_m and α_b are obtained from Eq. (1). Experimental results show that the bearing deformation capacity is sufficient to sum up the bearing resistances per bolt even in the case of small end distance e_1 and large bolt spacing p_1 [4,11]. For mild steel, the full characteristic bearing resistance of $3dtf_u$ (see Eqs. (1)–(2)) is related to the bearing deformation capacity at least equal to the bolt diameter $u = d$ [10].

Based on the new bearing deformation relationship, a design using prEN 1993-1-8 [3] has option to use two rules – the ductility rule and the bearing deformation rule. The boundary between the nominally elastic and plastic behaviour is 80% of the ultimate bearing resistance. The ductility, when it is provided by the bearing deformation, is assured if the shear resistance of bolt is greater than the 80% of the ultimate bearing resistance – the ductility rule. The bearing deformations at bolt hole are limited to the bolt hole deformations of $d/6$ when the bearing forces are lower than 80% of the ultimate bearing resistance, but not greater than $2\,f_u\,d\,t$, according to Eq. (11).

The net cross-section resistance represents the upper limit of a plate with holes in tension. New draft prEN 1993-1-1 [12] assumes, if no cracks exist at bolt hole [13], fully plastic and fully strain hardened design resistance of net cross-section is predicted by following formulae:

$$N_{u,Rd} = \frac{A_{net}f_u}{\gamma_{M2}} \tag{13}$$

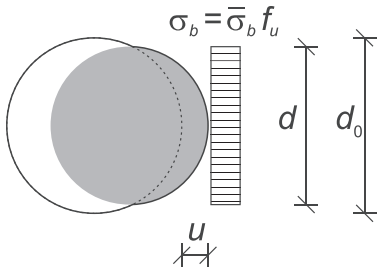

Fig. 2. Presentation of hole elongation and normalized bearing stress.

2. Experiments on double lap connections

An experimental program on bolted connections was carried out at TU Delft to (i) validate the new resistance models given in prEN 1993-1-8 on connections and (ii) validate the finite element model used to determine the load-bearing behaviour of various bolted connections considering material damage model and, where high local ductility is required.

Type A specimens are an inner plate of a double lap connection with two bolts specifically arranged perpendicular to the bearing force. Two different connection geometries type A with a plate width of 100 mm were chosen, and four tests were performed with each geometry. Specimens A1 and A2 have bolts positioned close to each other, while the bolts in specimens A3 and A4 are positioned close to the plate edge as shown in Fig. 4. The thickness of the inner and lap plates was the same.

Type B specimens also feature an inner plate of double lap connections with either 2 or 4 bolts arranged perpendicular to the bearing force, with a plate width of 240 mm. All connections are bolted with M12 12.9 bolts, which did not have any plastic deformation. The geometry of the test specimens is shown in Table 1 and in Fig. 4. Connections B1 and B2 have four bolts arranged in a line perpendicular to the bearing force, with a bolt spacing p_2 of 2.2 d_0, which is smaller than recommended by EC3, $p_2 = 2.4d_0$. The inner plates (test specimens) have very large end distances e_1 of 6 d_0 and 4 d_0 for B1 and B2, respectively, while the edge distance e_2 for both connections is 5.93 d_0. The lapping plates were also 6 mm thick and sufficiently dimensioned to preclude their failure and significant yielding. Fracture of the highly stressed area of the inner plate between the bolts is expected. Since the bolt spacing p_2 is small, a high local ductility of the material between the bolts was required to achieve the full bearing resistance. As described earlier, the full bearing resistance of $3f_udt$ develops when a large deformation of the bolt holes (approximately equal to the bolt diameter d) is achieved and the distances perpendicular to the bearing force are sufficient. This is clearly not provided by the connections B1 and B2.

Connection B3 has two bolts arranged in a row perpendicular to the direction of the force. The inner plate of the double lap connection has two widely spaced bolt holes ($p_2 = 16.06\ d_0$), located near the plate edge ($e_2 = 1.2\ d_0$) and far from the plate end edge ($e_1 = 26.9\ d_0$). The lapping plates of connection B3 were 10 mm thick designed to avoid their failure and to prevent significant yielding. The geometry of the connection indicates a fracture of the net tensile area between the plate edge and the bolt hole. In this case, the block tearing resistance calculated by Eq. (10) is not relevant due to the extremely large end distance e_1, while the bearing resistance model (see Eq. (1)) does not consider edge distance e_2. Similar to B2 and B3, a high local ductility of the net area is required to achieve the full bearing resistance. Therefore, in this case, a reduction of the bearing resistance considering Eq. (3) can apply. The lapping plates were in all cases sufficiently thick that the bearing deformations at bolt hole were insignificant compared to the deformation of the inner plate.

Displacement-controlled tests were performed in a servo-controlled universal testing machine at the prescribed speed of 1.7 mm/min. The relative displacements between the inner and lapping (cover) plates were measured using two linear variable displacement transducers (LVDTs). The LVDTs were placed on opposite sides of the B1 and B2 connection. They were positioned 20 mm from the centre of the outer bolt hole toward the vertical edge (see Fig. 5). The LVDTs measured the displacement between the centre of the bolt hole on the lapping plate and the position on the specimen that was 20 mm from the edge of the cover plate. For connection B3, both LVDTs were mounted on one side, as shown in Fig. 5. They measured the displacement between the centre

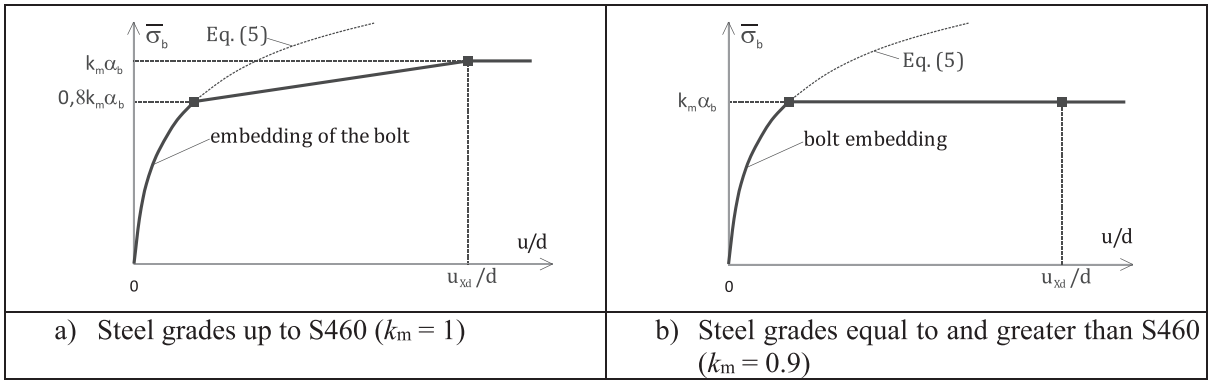

Fig. 3. Bearing deformation behaviour.

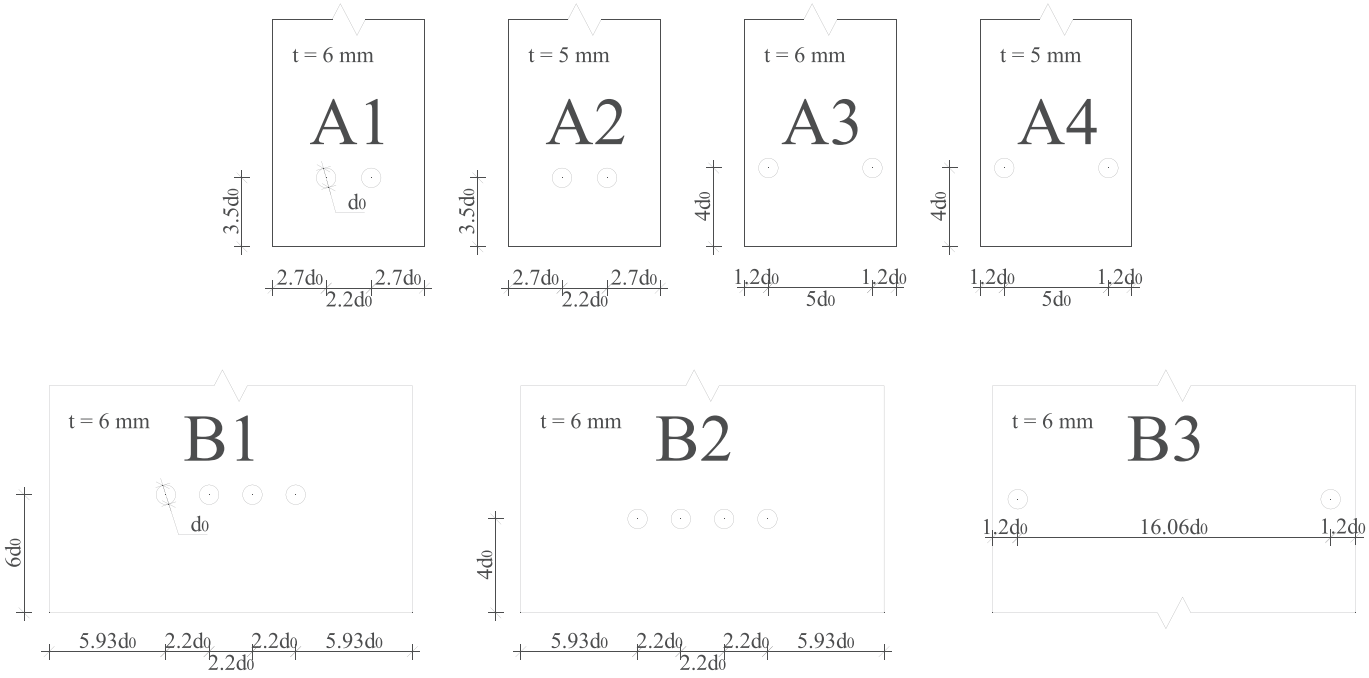

Fig. 4. Nominal dimensions of specimens for validation of the design provisions.

Table 1
Measured geometrical dimensions and material designations of bolted connection specimens.

Specimen	Material	No. of bolts	t [mm]	b [mm]	d_0 [mm]	e_1 [mm]	e_2 [mm]	p_2 [mm]	Specimen length [mm]
A1-1	M1	2	5.9	100.3	13.1	46.0	36.0	28.3	350
A1-2				100.4		45.7	35.9	28.6	350
A2-1	M2		5.4	99.4	13.4	45.2	35.8	27.8	350
A2-2				99.8		45.1	35.9	28.0	350
A3-1	M1	2	5.9	100.1	13.1	50.8	16.4	67.3	350
A3-2				100.3		50.8	16.5	67.3	350
A4-1	M2		5.4	99.6	13.4	49.7	15.9	67.8	350
A4-2				98.9		49.8	15.8	67.3	350
B1	M3	4	5.8	239.7	13.0	77.6	76.9/77.1	28.5/29.0/28.2	505
B2				239.3		52.1	76.9/77.1	28.5/28.8/28.0	505
B3		2		240.0		350	15.6	208.8	505

of the bolt hole on the lapping plate and the position on the specimen that was 60 mm from the edge of the cover plate. In this paper, the average value between both LVDTs is shown in the figures. The force was measured with a load cell that is integrated in the testing machine.

3. Finite element analysis

Several numerical models were created using the finite element software Abaqus [14] to validate the design rules imposed by the new Eurocode. The first series of numerical models refers to the numerical simulation of experiments on tensile and shear specimens (see Fig. 6) to

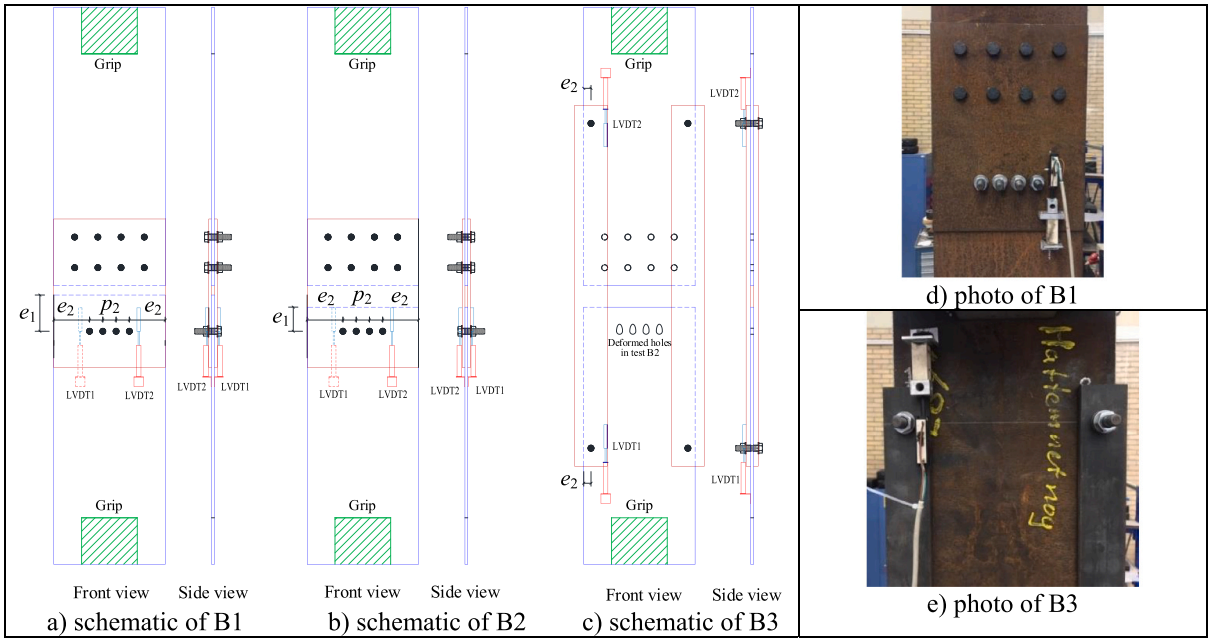

Fig. 5. Schematic and tests of connection series B.

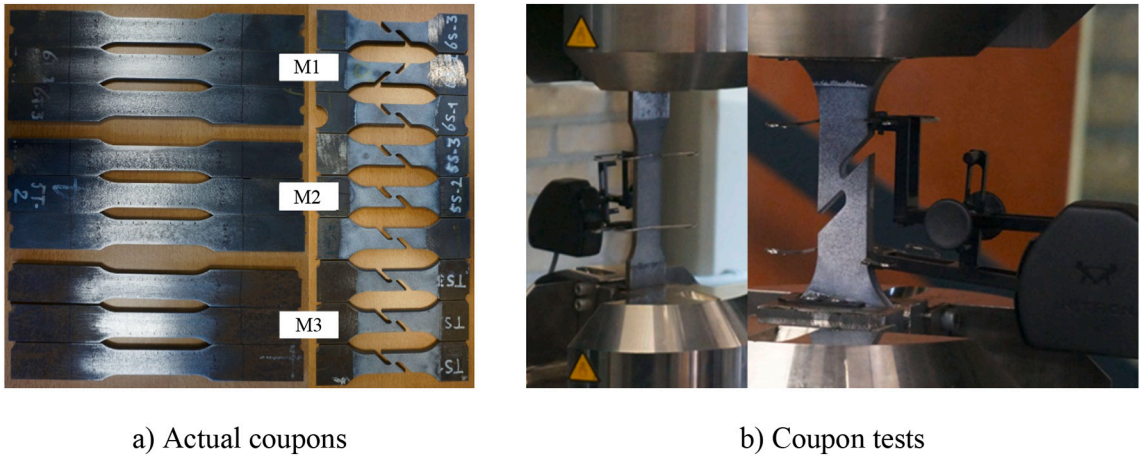

Fig. 6. Tensile and shear coupon tests.

calibrate the material model, considering damage initiation and fracture evolution law. The second series of numerical analysis simulates the experiments on bolted connections carried out in the Stevin II laboratory at TU Delft, which were used to validate the numerical models of connections. In the third numerical series validated FE models were used to analyse bolted connections with specific geometry and bolt arrangement of the numerical analysis.

3.1. Material modelling

The material properties of different steel grades are listed in Table 2.

Table 2
Parameters for material models.

	f_y [MPa]	f_u [MPa]	W	C_1	C_2
M1	320	440	0.6	0.6	1.4
M2	330	450	0.5	0.6	1.4
M3 (S355)	375	517	0.2	0.7	1.4
S690	746	785	−0.3	0.7	1.4

The properties for mild steels were determined by standard tensile testing and by shear tests, which were performed on coupons to characterize shear fracture. Three coupons of each type were taken from each steel plate used to make the connections. The coupons are shown in Fig. 6, where the steel grades were labelled by M1, M2, and M3. In addition, the properties of high strength steel S690 that are shown in Table 2 referring to the literature [15]. The tensile and shear tests of mild steels were numerically simulated to calibrate the factors describing post-necking true stress-strain relationship and damage initiation criterion. The coupons were numerically modelled in Abaqus, with a mesh size of about 1 mm in the "critical" part of the coupon. The shear coupon was meshed with 40 elements in the longitudinal direction of the shear region, while there were 10 elements in the width direction of the shear coupon. The elastic-plastic material with isotropic hardening was defined by the elastic modulus of 210 GPa and Poisson's ratio of 0.3, and by the Mises yield criterion, which was described by the true stress-strain relationship. The true stress–strain relationship before necking is obtained from the engineering stress-strain relationship (σ_e – ε_e), which is a result of testing on the tensile coupons. The engineering

stress-strain relationship is converted to the true stress–strain relationship as follows:

$$\sigma_t = \sigma_e(1+\varepsilon_e) \tag{14}$$

$$\varepsilon_t = ln(1+\varepsilon_e) \tag{15}$$

After necking, the deformations are no longer evenly distributed along the gauge length. Therefore, a combined linear and power stress–strain law proposed by Ling [16] was used to describe the behaviour after necking, as expressed by Eq. (16). Yang and Veljkovic [17,18] extended the combined linear and power stress-strain law to describe the post-necking stress-strain relationships of high-strength steels with weighting factor less than zero:

$$\sigma_t = (W)(a\varepsilon_t + b) + (1-W)\left(K\varepsilon_t^n\right) \tag{16}$$

where $(a\varepsilon_t + b)$ is the linear stress law, $(K\,\varepsilon_t^n)$ is the power stress-strain law, and W is a weighting factor that must be calibrated. Since the stress continuity and initial necking conditions must be satisfied simultaneously, the following parameters can be derived: $a = \sigma_{t,u}$, $n = \varepsilon_{t,u}$, $b = a(1-n)$, and $K = a/n^n$, where $\sigma_{t,u}$ and $\varepsilon_{t,u}$ are the true stress and strain at the beginning of necking.

After calibrating the weighting factor W, a damage initiation criterion for the fracture can be calibrated. An example of the influence of the parameter W and the true stress-strain relationships are shown in Fig. 7. Stress triaxiality along with strain intensity, is the most important factor controlling the initiation of ductile fracture. The relationship between equivalent plastic strain at fracture and stress triaxiality can be described by three functions, where the slope can be discontinuous in the transition region. For negative stress triaxialities, fracture is determined by the shear mode. For large triaxialities, void growth is the dominant failure mode, while for low stress triaxialities between the above two regimes, fracture can develop as a combination of shear and void growth modes [19]. Since only tests characterising tensile and shear fracture were performed, a damage initiation criterion describing different failure modes with two parameters that can be calibrated to fit tensile and shear coupon test results, was selected. The equivalent plastic strain (PEEQ) at damage initiation given by the following equation is a function of stress triaxiality η, strain rate and two calibration factors C_1, C_2:

$$\bar{\varepsilon}_D^{pl}(\eta,\dot{\bar{\varepsilon}}^{pl}) = \begin{cases} \infty, \eta < -1/3 \\ \dfrac{C_1}{3\eta+1}, -1/3 \le \eta < 0 \\ (C_2 - C_1)(\eta/\eta_0)^2 + C_1, 0 \le \eta < \eta_0 \\ \dfrac{C_2}{\eta/\eta_0}, \eta_0 \le \eta \end{cases} \tag{17}$$

where $\eta_0 = 1/3$. The calibration factor C_1 is calibrated for shear fracture, while the factor C_2 is calibrated for tensile fracture, as shown in Fig. 8. The engineering yield stress f_y, tensile strength f_u and the final choice of calibration factors are presented in Table 2. The damage initiation criterion is satisfied when the damage variable reaches the value of 1:

$$\omega_D = \int \frac{d\bar{\varepsilon}^{pl}}{\bar{\varepsilon}_D^{pl}(\eta,\dot{\bar{\varepsilon}}^{pl})} = 1 \tag{18}$$

Once the damage initiation criterion is reached, the degradation rate of the material stiffness starts. The damage evolution law is introduced in ABAQUS [14] by a scalar damage variable D, which is a function of the effective plastic displacement $\bar{u}_i^{pl}$. The value of $\bar{u}_i^{pl}$ is defined by the following equation:

$$\bar{u}_i^{pl} = L_{char}\left(\bar{\varepsilon}_i^{pl} - \bar{\varepsilon}_D^{pl}\right) \tag{19}$$

L_{char} is the characteristic length of the finite element (for C3D8R it is assumed to be equal to the element edge length) and $\bar{\varepsilon}_i^{pl}$ is the equivalent plastic strain (PEEQ). The finite element is removed from the mesh as soon as it reaches the maximum degradation D_{max}. The damage evolution law is defined by the displacement type with a small displacement at failure to achieve the sudden fracture shortly after the damage initiation. The displacement at failure $\bar{u}_f^{pl}$ was set to be 0.01 mm, corresponding to the maximum degradation D_{max} equal to 1.0. Therefore, the damage initiation point can be regarded as the onset of fracture point. The fracture evolution in the analysis of bolted connections can be regarded as an approximation for the actual fracture failure since the considered damage evolution law is not accurate enough for the crack evolution analysis.

In this paper, FEA on bolted connection with mild steel S355 (M3 steel in Table 1) and high-strength steel S690 is considered.

The high strength M12 12.9 bolts used in the experiments were designed not to fail. Nevertheless, a linear-elastic and parabolic-plastic stress-strain relationship was assumed for the pre-necking stress-strain curve, with the vertex of the parabola corresponding to the ultimate

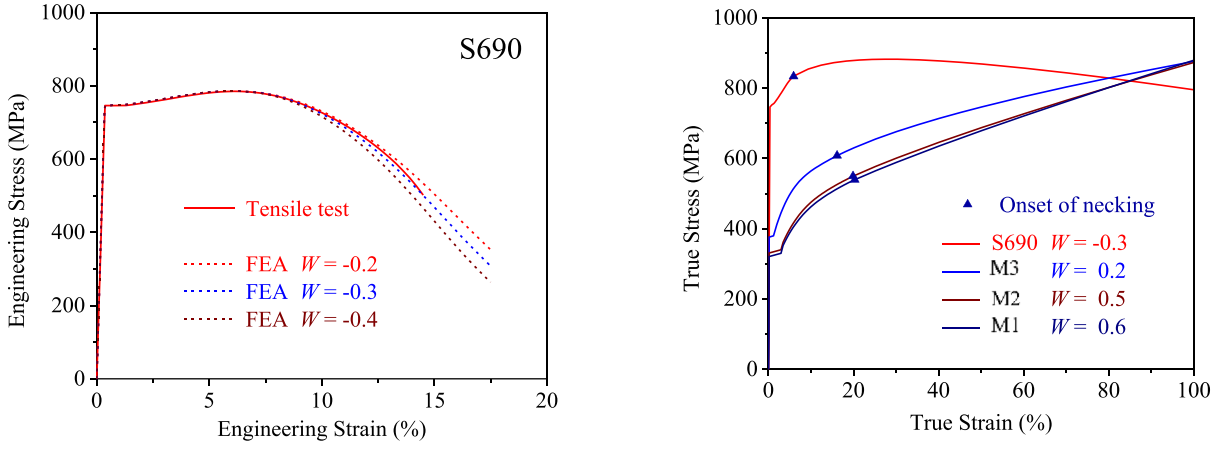

a) calibration of W for S690 steel

b) true stress-strain relationships

Fig. 7. Stress-strain diagrams.

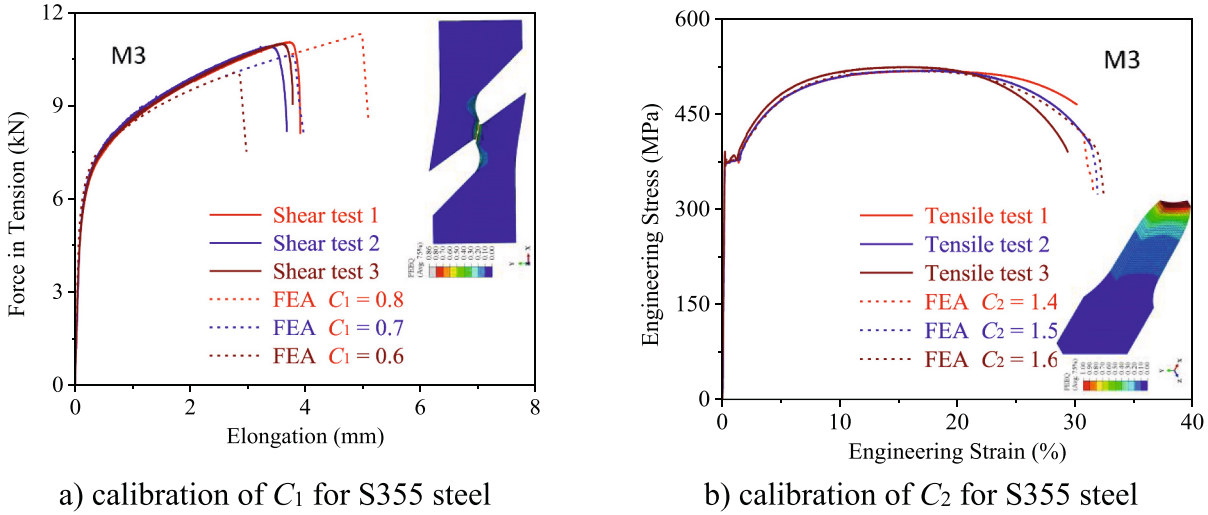

a) calibration of C_1 for S355 steel b) calibration of C_2 for S355 steel

Fig. 8. Calibration parameters for damage initiation criteria.

strength of the bolt material. The nominal yield strength of 1080 MPa and the nominal ultimate strength of 1200 MPa were used to determine the stress-strain curve, and the engineering strain corresponding to the ultimate strength was assumed to be 0.05. Detailed information about the true stress-strain relationship after necking described by the power law can be found in [20]. Both numerical analysis and experiments showed insignificant plastic yielding of the bolts.

3.2. Numerical simulation of tests on bolted connections

The numerical models of the double lap connections were composed of two plates overlapping the inner plate and connected by bolts (Fig. 9a)-c)). The model of the bolts considered the geometry of the hexagon bolt head and nut, the threads, and the washers placed under the head and nut (Fig. 9d)). Abaqus general formulation of the contact was prescribed between the plates and between the bolt and the plate, using the "hard" behaviour in the normal direction and the friction formulation with the coefficient of 0.1 in the tangential direction. For meshing of the plate, 8-node reduced integration C3D8R solid elements with an edge length in the region of interest of about 1.0 mm were used. The problem was solved using the explicit solver with a time step of 200 s and a target increment of 0.002 s.

In order to reduce the computational cost, quarter finite element models were created for the series A and B connections, considering two symmetry planes for these models. The symmetric boundary conditions about the Y-axis (see Fig. 9) were applied to the bottom surfaces of the two lapping plates. The symmetric boundary conditions about the X-axis were applied to the right surfaces of the two cover plates and the inner plate. A reference point was defined directly above the symmetry plane of the middle plane, to which the nodes of the upper surface of the inner plane were coupled with all degrees of freedom (DOFs). A displacement in the positive Y-axis was applied to the reference point, while the other DOFs were constrained. The boundary conditions of FEA1 were defined in the same way.

For the FEA2 connections, all DOFs of the nodes of the right surfaces of the two lapping plates were coupled to the reference point located at their centre (see Fig. 11b). Similarly, the left surface of the inner plate was coupled to the reference point to which a rotation about the *Z*-axis was applied to simulate the bending moment. The other DOFs of the reference points were constrained. In addition, the displacements of the inner plate about the Z-axis were constrained to avoid instabilities.

The history of displacements was generated from the nodes corresponding to the measurements of displacements by LVDTs. The numerical results showed that these displacements practically coincided with the bearing deformation of the bolt hole.

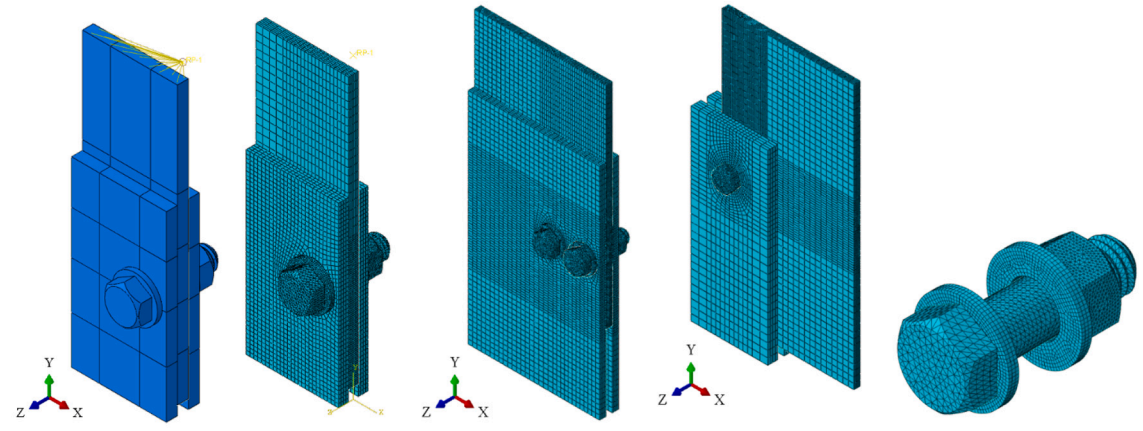

a) type A connection assembly b) B1and B2 connection assembly c) B3 connection assembly d) model of bolt assembly

Fig. 9. Presentation of finite element models.

3.3. Validation of the numerical models of connections

The numerical model with the material model developed on the experimental results of the shear and tensile coupons was validated with the experimental results of the bolted connections A1 to A4 and B1 to B3 described previously. The failure modes shown in Fig. 10 demonstrate that the numerical model predicts the deformation behaviour and location of the fracture well. The failure modes of the connections not shown (A2, A4, B1) are the same as those shown. The load displacement curves obtained experimentally and numerically are presented in Section 4, while the summary and comparison of experimental and numerical results can be found in Table 3. The numerical and experimental resistance agree well with a maximum error of 4%, while the displacement at maximum failure is overestimated by 32% on average. However, the shape of the load displacement curves agrees very well (see Figs. 12, 14, 15, 17). Better results could be obtained if more coupon tests were performed of different stress triaxialities to better describe the fracture locus.

3.4. FEA of connections for validation of design provisions

Numerical models of bolted connections with three geometries and two steel grades S355 and S690 (see Table 2) were created to validate the design rules in the new prEN 1993-1-8 [3]. The conceptual design of numerical models is described in 3.2, above.

"Connection FEA1" model is a double lap connection with four bolts positioned as shown in Fig. 11a, where symmetry boundary conditions were considered. Mid-plate has a group of widely spaced between them, but bolt rows are near the plate edge and far from the plate end edge. The objective of the numerical analysis of this connection is to show whether its available deformation capacity is sufficient to develop the full bearing resistance according to Eq. (1), or the resistance must be reduced because of the fracture of the highly stressed net area. The connection is designed so that the block tearing resistance is greater than bearing resistance of the bolt group. The connection is analysed considering ductile mild steel S355 and high strength steel S690 which has much lower ductility in terms of tensile to yield ratio, uniform deformation, and fracture deformation.

"Connection FEA2" model is also a double lap connection with 8 bolt rows with a single bolt in a row subjected to a bending moment (Fig. 11b). As Eurocode allows elastic and partial/full plastic distribution of forces between bolts, the question is whether the local ductility is sufficient to allow fully plastic distribution of forces. In the notation of these connections in Table 4 FEA2-*xx-p/i*, *xx* represents the end distance in mm, while *p* represents perfect alignment of the and bolt holes and *i* represents imperfect alignment of the bolt holes. The bolts in the perfect alignment are in the center of the bolt holes and all bolt holes in the inner and cover plates have the same transverse position. Therefore, clearances exist in all the bolt holes and the double lap connection starts carrying a bending moment after a certain rotation when bolt shanks get in contact with the bolt hole walls. When the bolt holes are imperfectly aligned, bolt holes 1 and 4 of the inner plate and cover plates are displaced for 1 mm to the opposite sides. Accordingly, there is no clearance and they immediately start transmitting the bearing pressure when the

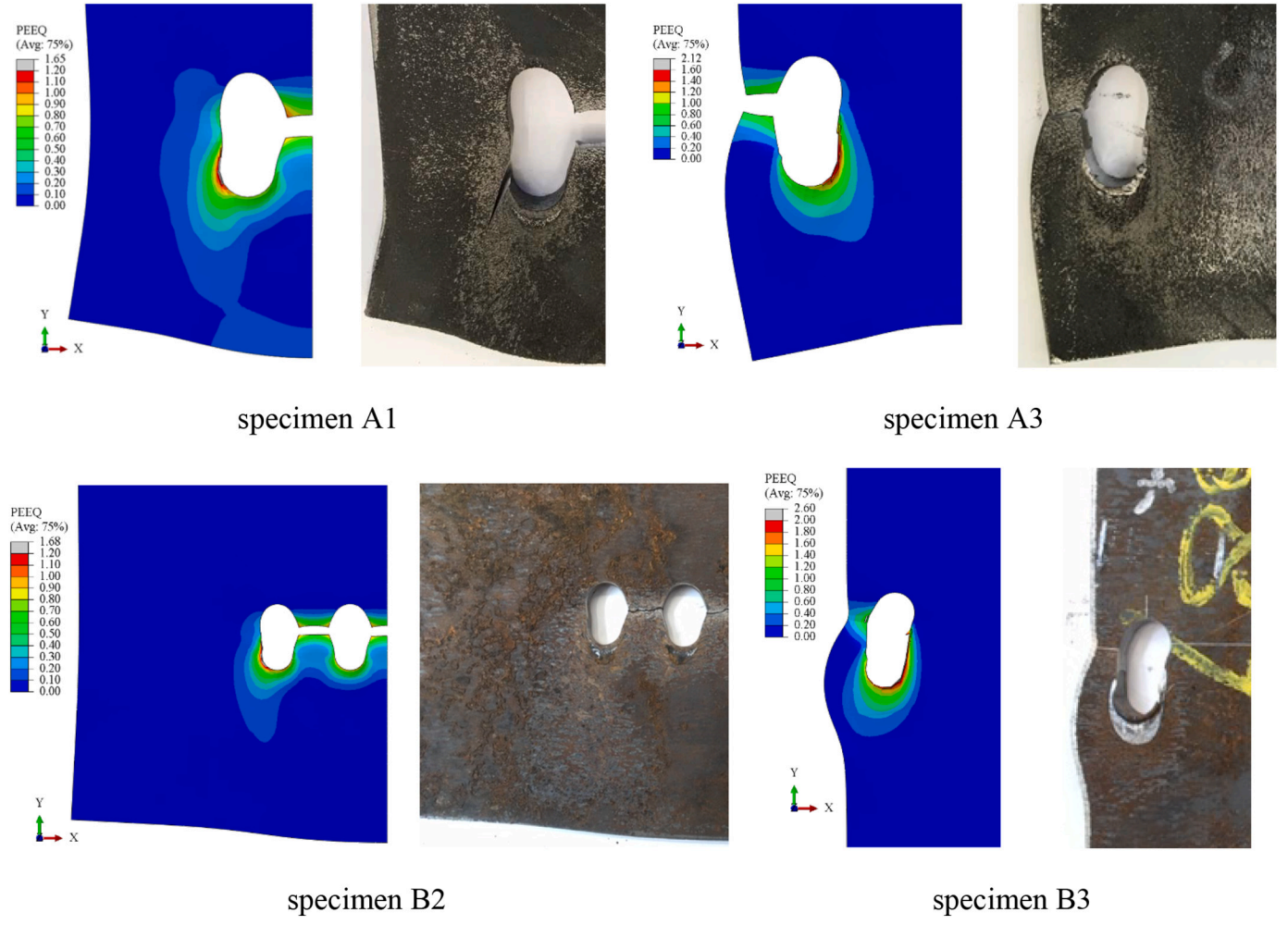

Fig. 10. Failure modes of connections A1, A3, B2 (one half of the specimen) and B3 (detail at bolt hole).

Table 3
Comparisons of experimental and numerical results.

Specimen	Maximum resistance				Corresponding displacement			
	Test [kN]		FEA [kN]	Ratio	Test [mm]		FEA [mm]	Ratio
A1-1	162.4	162.4	167.3	103%	10.1	9.0	11.8	131%
A1-2	162.5				7.9			
A2-1	149.2	149.1	150.6	101%	7.9	8.1	11.1	137%
A2-2	148.9				8.2			
A3-1	–	182.7	181.4	99%	–	10.4	13.9	135%
A3-2	182.7				10.4			
A4-1	156.3	157.3	163.3	104%	9.0	9.2	12.8	139%
A4-2	158.4				9.4			
B1	391.8		395.4	101%	8.0		9.5	119%
B2	325.8		326.1	100%	6.0		7.9	133%
B3	277.2		278.4	100%	14.2		18.3	129%

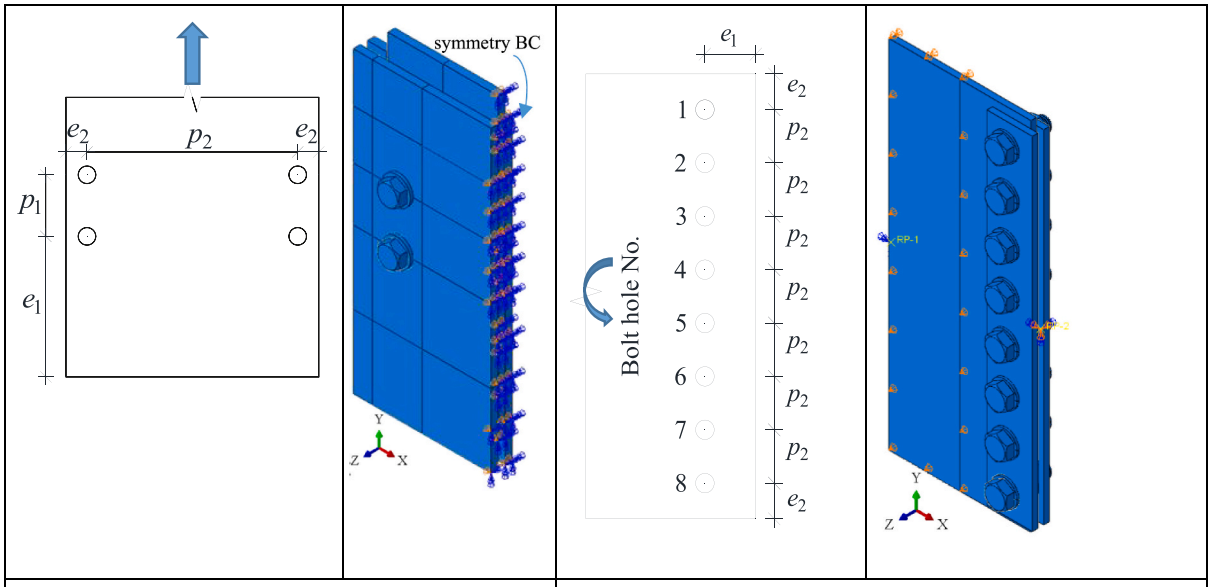

a) specimen and FEA1 model – group of distantly spaced bolts close to the plate edge and far from the plate end edge

b) specimen and FEA2 model – bolt group loaded by a bending moment

Fig. 11. Connections for validation of design provisions.

Table 4
Geometry of connections used in FE parametric study.

Connection	No. bolts	t [mm]	d [mm]	d_0 [mm]	e_1/d_0	p_1/d_0	e_2/d_0	p_2/d_0	Width [mm]	Height [mm]	f_y [MPa]	f_u [MPa]
FEA1-S355	4	6	12	13	8	3.8	1.2	12	93.6/117	253.5/253.5	375	517
FEA1-S690											746	785
FEA2-27p-S355	8	8	20	22	1.23	/	1.82	2.73	200/64	500/480	375	517
FEA2-27p-S690											746	785
FEA2-27i-S355											375	517
FEA2-27i-S690											746	785
FEA2-66p-S355					3						375	517
FEA2-66p-S690											746	785
FEA2-66i-S355											375	517
FEA2-66i-S690											746	785

The width and the height correspond to the dimensions of the inner/lapping plates.

bending moment is applied. The remaining bolts are positioned as in the situation with perfect alignment. In this way, the ductility requirements for bolt hole 1 are larger at the imperfect alignment than in the perfect alignment.

4. Validation of EC3 design rules on connections

4.1. Connection types A1 to A4

Connection types A1 to A4 failed in block tearing, showing a large

deformation due to the bearing action at the bolt hole. Tensile failure of the plate between the bolt holes was observed in series of connections A1 and A2, while tensile failure between the bolt hole and the edge characterized connections A3 and A4 (see Fig. 10). The load-displacement curves are shown in Fig. 12, where the experimental, numerically simulated and prediction curves are plotted. The experiment of A3-1 failed due to an equipment failure. The new prEN 1993-1-8:2021 allows prediction of load deformation behaviour due to bearing action. The non-dimensional average bearing stress for a single bolt is obtained from Eq. (11), where u is the bolt hole deformation and d is the bolt diameter ($d = 12$ mm). The bearing force is calculated as:

$$F_b(u) = \overline{\sigma}_b(u) d t f_u \tag{20}$$

The connection is utilized by two lapping 6 mm thick plates and the number of bolts $n_b = 2$. Visual observation of the bearing deformation of lapping plates and the shear deformation of the bolt showed insignificant deformation of these components. Therefore, they can be neglected, which simplifies the calculation of the deformation behaviour. Thus, the connection resistance $R(u)$ is a function of the bearing deformation at all holes:

$$R(u) = n_b F_b(u) \tag{21}$$

Since the maximum resistance is governed by the block tearing resistance according to Eq. (10) (calculated without the partial safety factor), the prediction curves in Fig. 12 follow Eq. (21) up to the block tearing resistance. It can be observed that the prediction curve follows the nonlinear behaviour in terms of bearing action very well. The maximum resistance that is governed by the block tearing resistance is underestimated by about 14% for specimens A1, A2 and by approximately 11% and 6% for specimens A3 and A4, respectively. Table 5 shows the resistances calculated according to the 2005 and 2021 versions of EN 1993-1-8. The values were calculated with measured geometric and material parameters and without the partial safety factors. It is interesting to observe that the bearing resistance is decisive for the design according to EN 1993-1-8:2005, which leads to significant underestimation of the experimental resistances by 38% to 53%.

4.2. Connections with specific arrangement of bolts

4.2.1. Group of closely spaced bolts far from the end plate edge

Connection types B1 and B2 fractured in the net tension area between the bolts as shown in Fig. 13. The closely spaced bolts interact, creating the stress critical zone around the bolt group while the width of the plate was sufficient to prevent yielding of the net cross-section. The yielding of the shear planes allowing large tensile deformations between the bolts, pushing out the block of material. Therefore, the failures are classified as the block tearing failure with large bearing deformations at bolt holes. The visual observations in Fig. 13 shows that the bearing deformations are more pronounced in the case of B1 on account of larger end distance e_1, which increased the resistance of B1 compared to B2.

The connection geometries with large end distance $e_1 > 3d_0$ were designed to provide full bearing resistance according to Eq. (1) and relatively high block tearing resistance according to Eq. (10). Since the ultimate resistance of these connections depends mainly on the deformation capacity of the steel between the bolts, the predicted resistances may be higher than the experimental one (unsafe). The calculation of

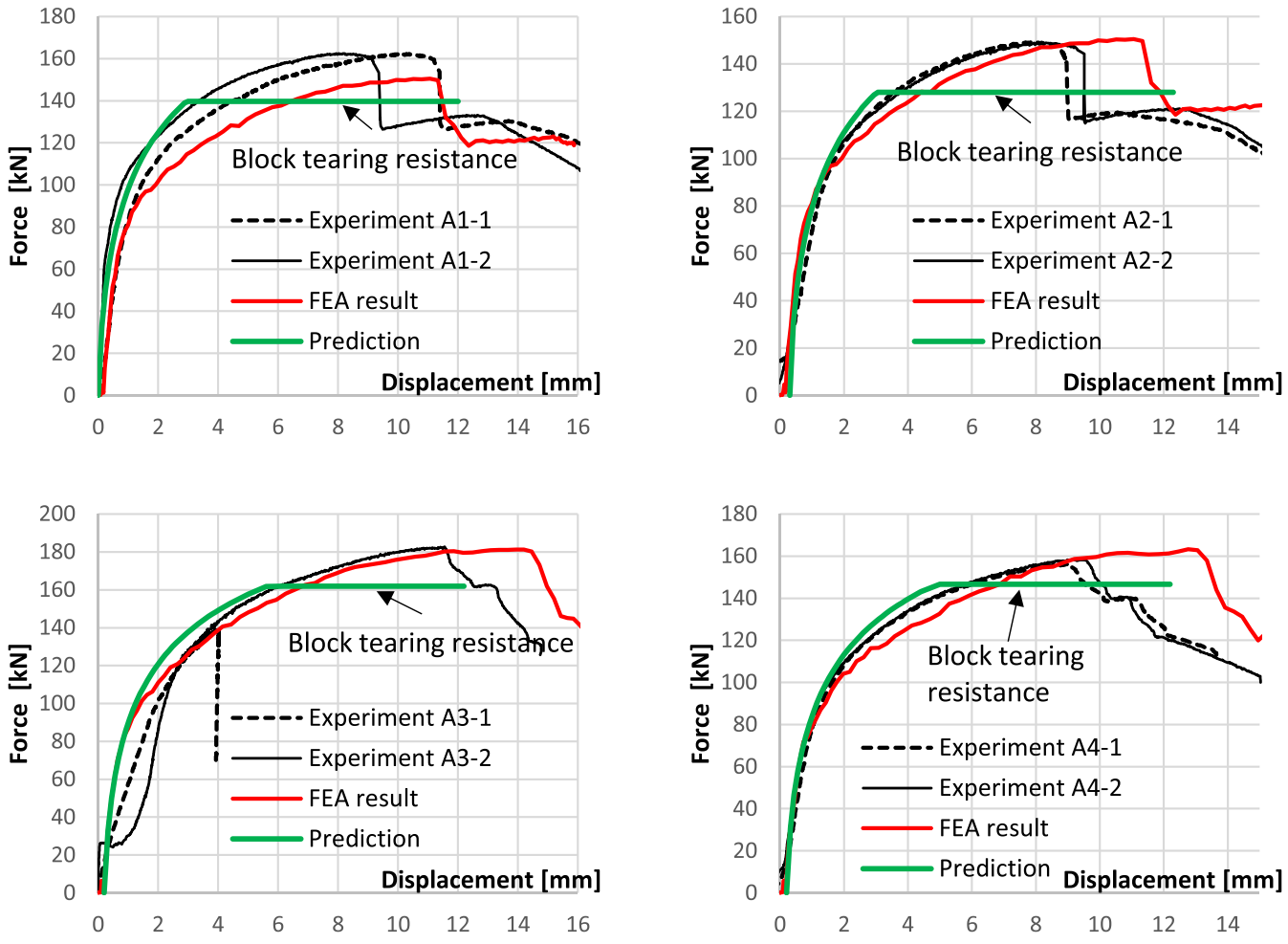

Fig. 12. Load displacement curves of connection types A.

Table 5
Resistances of connections A according to of EN 1993-1-8, versions 2005 and 2021.

Specimen	A1-1	A1-2	A2-1	A2-2	A3-1	A3-2	A4-1	A4-2
$F_{u,exp}$ [kN]	162.4	162.5	149.2	148.9		182.7	156.3	158.4
prEN 1993-1-8:2021								
F_b [kN]	93.5	93.5	87.5	87.5	93.5	93.5	87.5	87.5
ΣF_b [kN]	186.9	186.9	175.0	175.0	186.9	186.9	175.0	175.0
V_{eff} [kN]	**139.7**	**139.9**	**128.0**	**128.3**	**161.9**	**162.4**	**147.0**	**146.7**
EN1993-1-8:2005								
F_b [kN]	41.3	42.3	35.1	35.7	56.2	56.9	47.3	46.7
ΣF_b [kN]	**82.5**	**84.5**	**70.2**	**71.5**	**112.5**	**113.8**	**94.6**	**93.4**
V_{eff} [kN]	125.5	125.6	114.2	114.5	147.6	148.1	133.2	132.9

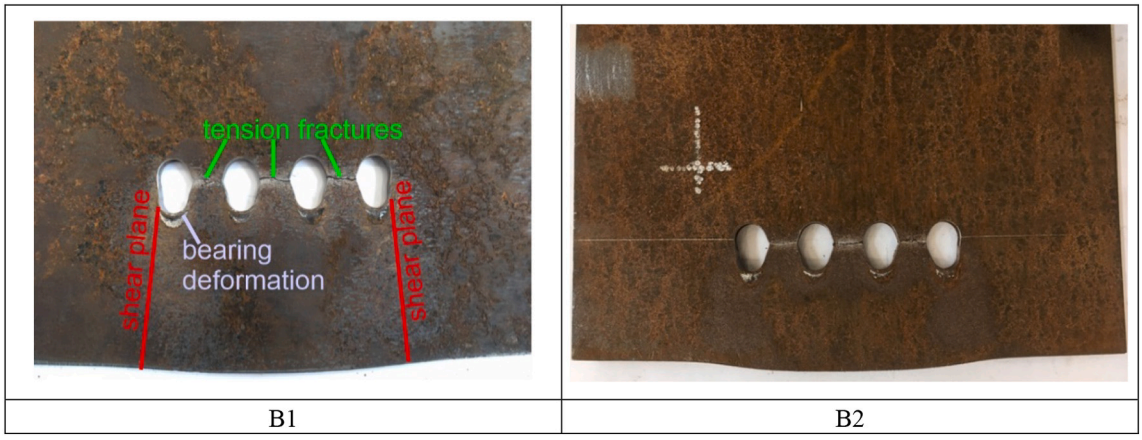

Fig. 13. Failures of specimens B1 and B2.

resistances presented in Table 6 shows that the block tearing resistance according to the new prEN 1993-1-8:2021 governs for both connection types. The block tearing resistance is well predicted for both connections.

The calculation according to EN 1993-1-8:2005 leads to a significantly lower predicted resistance, where the bearing resistance is decisive for the design. The experimental resistance is greater than the predicted resistance by a factor of 2.02 and by 1.68 for B1 and B2, respectively. This conservatism results from the reduction factor for small bolt spacing p_2, which is considered in EN 1993-1-8:2005. The characteristic resistances in Table 6 are calculated with the measured parameters.

Fig. 13 shows the failures of specimens B1 and B2, while Figs. 14 and 15 show the experimental response curve and the predicted curve by assuming only the bearing deformation according to Eq. (21). Fig. 14 shows that the experimental load-deformation curve for B1 is well predicted, while the prediction of B2 agrees with the experimental curve in the initial stage and it is slightly overestimated from a displacement of more than 1 mm. As explained earlier, the bearing deformation is more pronounced for B1. The shear planes of B2 start to yield at lower force than of B1, decreasing the stiffness on the account of shear deformation in the shear planes and the tensile deformations between the bolts. The predicted curve is truncated when the block tearing resistance it reached

Table 6
Resistance of connection types B1 and B2 according to EN 1993-1-8, versions 2005 and 2021.

Connection type	B1		B2	
Version of EN 1993-1-8	2005	2021	2005	2021
$V_{eff,1}$ [kN]	316	333	252	268
ΣF_b [kN]	194	432	194	432
$F_{u,exp}$ [kN]	392	392	326	326
F_u/ min ($\sum F_b$; $V_{eff,1}$)	2.02	1.18	1.68	1.21

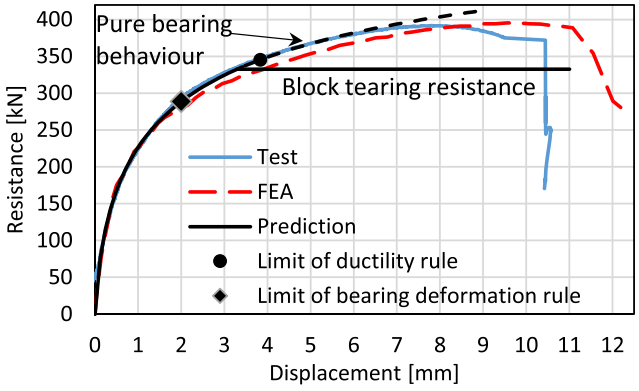

Fig. 14. Load deformation curves of B1.

(see Table 6). The dashed lines in Figs. 14 and 15 represent the prediction of pure bearing behaviour, i.e., when the bolt spacing p_2 would be sufficient to prevent the block tearing failure. The limit of bearing deformation and the ductility rules are also presented. If connections B1 and B2 were designed in compliance with bearing deformation rule (i.e. the bearing resistance is limited to $F_u = 2dtf_u$), their analytical resistance would be limited to 288 kN. In fact, at 288 kN, the deformations are limited to 2 mm (excluding the initial slip), as shown in Fig. 14. The resistance of connection B2 according to prEN 1993-1-8:2021 is defined by the block tearing resistance, which is equal to 268 kN (see Table 6), and therefore smaller than 288 kN, which makes the bearing deformation and the ductility rule irrelevant. It can be seen from Figs. 14 and 15 that the numerical analyses considering the calibrated stress-strain relationships and damage criterion would simulate the behaviours of B1 and B2 connections well, especially for the initial load-displacement curves and the ultimate bearing resistance, see Table 3. The

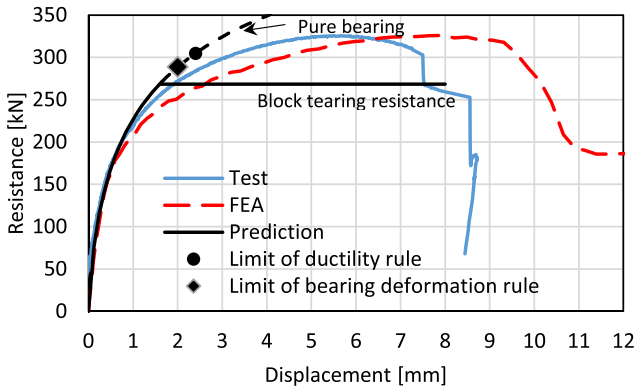

Fig. 15. Load deformation curves of B2.

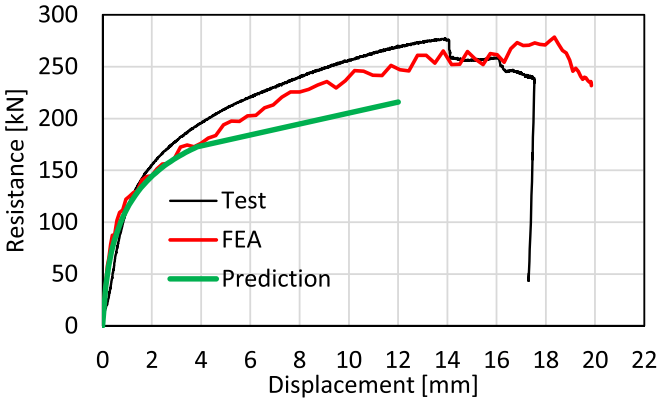

Fig. 17. Load deformation curves of B3 specimen.

displacements corresponding to the ultimate resistance are overestimated since the damage criterion used is calibrated only based on tensile and shear coupons. The damage criterion needs to be improved for more accurate predictions.

4.2.2. Group of widely spaced bolts near the plate edge and far from the plate end edge

Connection type B3 and FEA1 are specific because the bolts are positioned very close to the plate edge parallel to the bearing force, while the end distance e_1, the bolt spacings p_1 and p_2 are large. Therefore, the maximum resistance depends mainly on the available local ductility of the net tension area adjacent to the edge.

The end distance e_1 of B3 is so large that the block tearing failure cannot occur. B3 specimen fails due to the fracture of the net tension area adjacent to the edge. As it can be seen in Fig. 16, the deformation capacity of the tension area was sufficient to develop a high bearing resistance and deformation, while the tensile stresses redistributed toward the center of the plate (away from the edge). Although the bearing force was applied parallel to the edge, the movement of the bolt toward the edge can be clearly seen in Fig. 16. The experimental and predicted load-displacement curves are shown in Fig. 17. The experimental curve shows a nonlinear behaviour, where the fracture of the net tension area interrupts further increase of the resistance. The predicted curve describes the bearing behaviour according to the behaviour described in the Introduction. The first part of the curve, describing the embedding of the bolt was obtained by Eq. (21) with the number of bolts $n_b = 2$. The embedment carries out up to 80% of the maximum bearing resistance, which is given in Table 7. The linearly increasing part describes the progression of yielding and reaches the maximum bearing resistance when the bolt hole deformation is 12 mm. Since the lapping plates were much stiffer than specimen B3, the bearing deformations of the lapping plates were not considered. The initial part of the predicted curve, which represents the embedment of the bolt, is in great agreement, while there is some reserve in the maximum resistance on the account of very large end distance. Since only one experiment was conducted with one mild steel grade, the reduction was proposed by considering Eq. (3). It shows a very conservative result. As mentioned earlier, this reduction should discourage designers from designing connections with bolts near the edge in combination with large end distances and bolt spacing. Table 7 shows a clear conservatism of the bearing resistance according to EN 1993–1-8:2005.

Fig. 18 shows equivalent plastic deformations (PEEQ) at maximum resistance and after fracture of FEA1 for steel grades S355 and S690, where only the area around the bolt holes is shown. The magnitude and distribution of the PEEQ at maximum resistance is similar, although the strain is more localized in the net region in the case of the mild steel S355, while a higher localization is observed in the bearing region in the case of the high strength steel. Fig. 19 shows the response curves for FEA1. The point A shows the initiation of the fracture in both diagrams of Fig. 19. It can be observed that the high strength steel is characterized by a shorter load deformation path from point A to point B, which represents the maximum resistance. After reaching the maximum resistance, the fracture progresses and the resistance decreases. Since the response is characterized by the bearing, the numerical curve can be compared with the analytical curve. Since the deformation of the lapping plates and bolts was insignificant, the analytical curve was obtained by Eq. (21) with the number of bolts $n_b = 4$, assuming the same deformation of all bolt holes. The analytical curves predict the numerically determined behaviour very well. The end of the predicted curve represents the bearing deformation at maximum resistance (see Eq. (12)) that quite corresponds to the maximum resistance observed in the

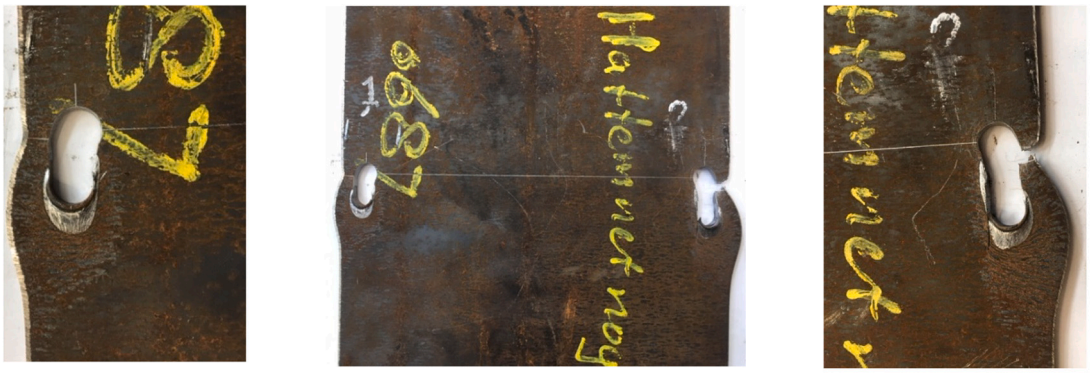

a) detailed view of the left hole b) fractured specimen B3 c) detailed view of the right hole

Fig. 16. Failure of B3.

Table 7
Resistances of B3 and FEA1 according to EN 1993-1-8, versions 2005 and 2021.

Units kN		B3				FEA1-S355				FEA1-S690			
EN 1993-1-8:		2005		2021		2005		2021		2005		2021	
$V_{eff,1}$	$F_u/V_{eff,1}$	/	/	/	/	394.2	1.13	444.9	1.00	757.6	0.76	792.7	0.73
ΣF_b	$F_u/\Sigma F_b$	123.6	2.24	223.3	1.24	236.9	1.87	446.7	0.99	359.7	1.60	610.4	0.94
ΣN_u	$F_u/\Sigma N_u$	/	/	112.9	2.46			225.8	1.96			342.9	1.68
F_u		277.2				443.5				575.2			

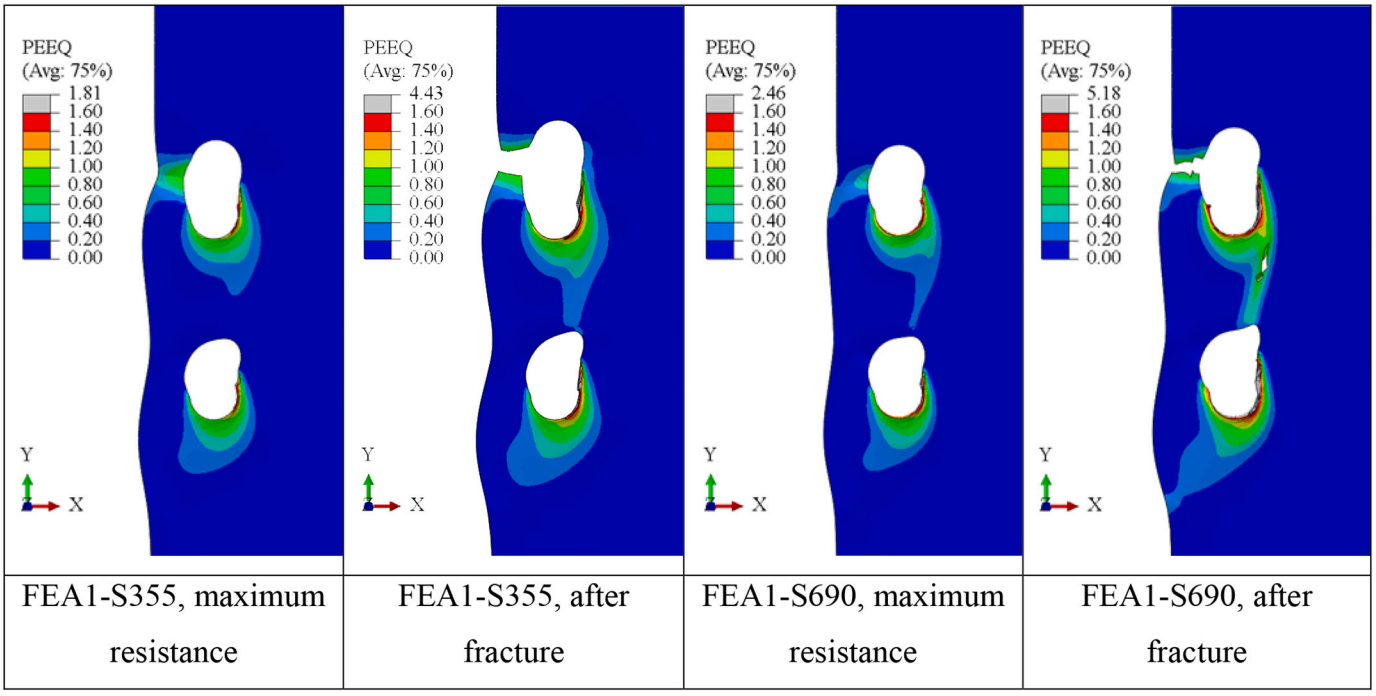

Fig. 18. Equivalent plastic deformation of FEA1.

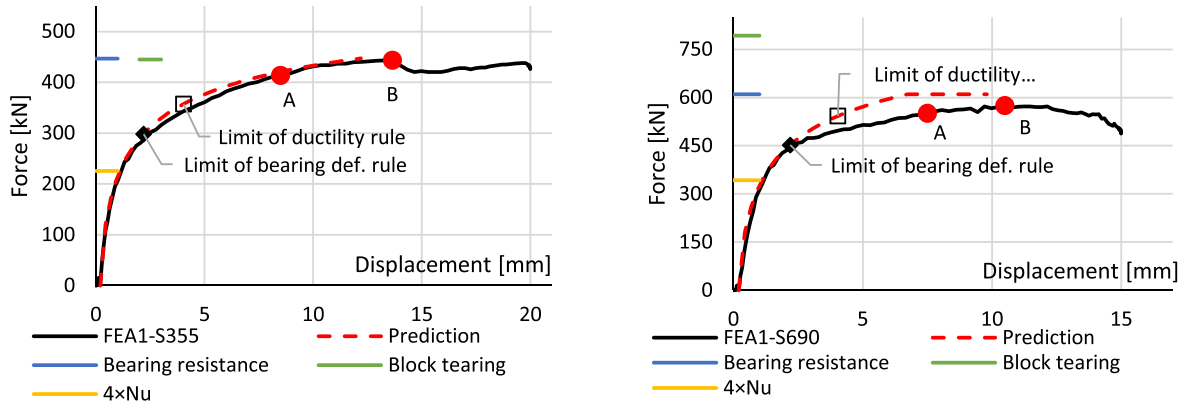

Fig. 19. Load deformation curves of FEA1.

FEA. If the connections were designed according to bearing deformation rule, the deformations would be limited to $d/6$. The limit of the ductility rule shows that the bearing deformations are indeed starting to increase significantly after 80% of the full bearing resistance is reached.

The resistance obtained according to the two versions of EN 1993-1-8 show that the bearing resistance model of the 2005 version is very safe with a factor of 1.87 for steel S355 and 1.60 for steel S690, where the bearing resistance is calculated as the sum of the bearing resistances at the individual bolt holes (the partial factors were not considered). The bearing resistance model according to the new version of the standard accurately predicts the numerical resistances. For S355 steel, the prediction is very accurate, while for steel S690, the resistance is overestimated by 6%. The bearing resistance is the governing check for the design in all cases. In the absence of the experimental results to confirm the numerical analysis, the reduction of bearing resistance was proposed by considering Eq. (3). The reduced resistance similarly underestimates the maximum numerical resistance as EN 1993-1-8:2005.

4.3. Bolt group loaded by a bending moment

Connection type FEA2 represent a web in bending with 8 bolts arranged in a column. Two geometries with an end distance of 26 mm and 66 mm, two steel grades S355 and S690, with perfect and imperfect bolt alignment were analysed (see Fig. 11b, Table 4). The results of the numerical analysis are shown in Figs. 20 to 23, where the equivalent plastic strain on a deformed shape at maximum resistance and after fracture is shown. Figs. 24 and 25 show the moment rotation curves, where the thicker curves represent the moment from the reaction at the reference point and the thinner curves represent the moment calculated from the contact forces on the bolts. The difference between the thick and thin curves observed at higher resistance is due to the frictional forces, since the frictional behaviour between surfaces was considered with the friction coefficient of 0.1. A small part of the difference between the curves is due to the unbalanced bearing force (see Table 8), which is the consequence of the automatically generated artificial energy of the finite element analysis using explicit solver. The bending moment, shown in thin curves, was calculated from the contact forces, assuming the origin of the coordinate system in the centre of the bolt group, as shown in Fig. 26. The moment rotation curves show that imperfect bolt alignment lowers the maximum resistance and initial stiffness. The reduction in maximum resistance is more pronounced for shorter end distance and higher steel grade (11% for FEA2-27-S690, 7% for FEA2-27-S355), while the connections with 66 mm end distance show only a 3% reduction regardless of steel grade. These results were expected since the plastic plateau due to the bearing action is shorter for small end distances and high strength steel. The evolution of the contact forces with perfectly and imperfectly aligned bolt holes for FEA2-27-S690 is shown in Fig. 27, where it can be observed that the contact force on bolt 1 is already decreasing when the contact force on bolt 3 reaches its plateau. However, similar failure was observed regardless of the bolt hole alignment. The connection with $e_1 = 26$ mm reached its maximum resistance when the bearing resistance of bolts 1 to 3 was fully utilized and failed when bolt 1 sheared out. The connection with $e_1 = 66$ mm reached its maximum resistance when the plate yielded in front of the bolt and in the tensile stressed area A_{nt}. The fracture started between bolts 1 and 2. In all cases, a large hole deformation due to the bearing action can be observed in all cases. Bolt holes 1 to 3 show similar deformation at maximum resistance. The deformation at bolt hole 4 lags behind the deformations of the upper holes and shows some bearing resistance. The centre of rotation is at bolt hole 5 ($F_5 = 0$, see Table 8), which is below the centre of the bolt group, because the force at the lower bolts points away from the plate edge, where the plate has larger resistance. The deformation and the bearing resistance at bolt hole 6 is small for FEA2-27 connections, while bolt hole 6 shows significant bearing resistance for FEA2-66 connections. The lower two bolt holes 7 and 8 show significant deformation with large bearing resistance. The distribution of forces between the bolts at maximum bending resistance is shown in Table 8 and Fig. 28.

Eurocode 3 part 1–8 [1,3] allows a linear elastic, elastic-partial plastic or fully plastic distribution of the forces between the bolts. If a linear-elastic distribution is assumed, the forces on bolts should be proportional to the distance from the centre of rotation. For plastic distribution, any equilibrium distribution is acceptable, provided the resistances of the components are not exceeded and the ductility of the components is sufficient. The centre of rotation is assumed to be at the centre of the bolt group. The following force distributions are assumed, shown in Fig. 26: elastic distribution (E), elastic-partial plastic distribution with two (EP2) or three (EP3) bolts reaching plastic resistance, and fully plastic distribution (FP).

The bending resistance of the connections was determined according to prEN 1993-1-8 [3] as follows. Possible failure modes and the design equations that describe the failure mode were identified for each force distribution. For the elastic distribution, the plate at bolt hole 1 can fail due to bearing action or due to L-shaped block tearing. For the distributions EP2, EP3 and FP, the failure due to the bearing action, L-shaped and U-shaped block tearing are possible and are given in Fig. 26. Hence, the maximum resistance of the bolts reaching plastic resistance is the smaller value of the bearing resistance obtained given by Eq. (1) and the block tearing resistance given by Eq. (10), divided by the number of bolts reaching plastic resistance. The partial factors are not considered. The bearing resistance and block tearing resistance are shown in Table 9. Forces on bolts and bending resistance for all force distributions are shown in Table 10. Assuming the centre of rotation is located the centre of the bolt group and equality of forces above and below the centre of rotation, the bending moment is calculated as:

$$M = 2\sum_{i=1}^{4} F_i r_i \tag{22}$$

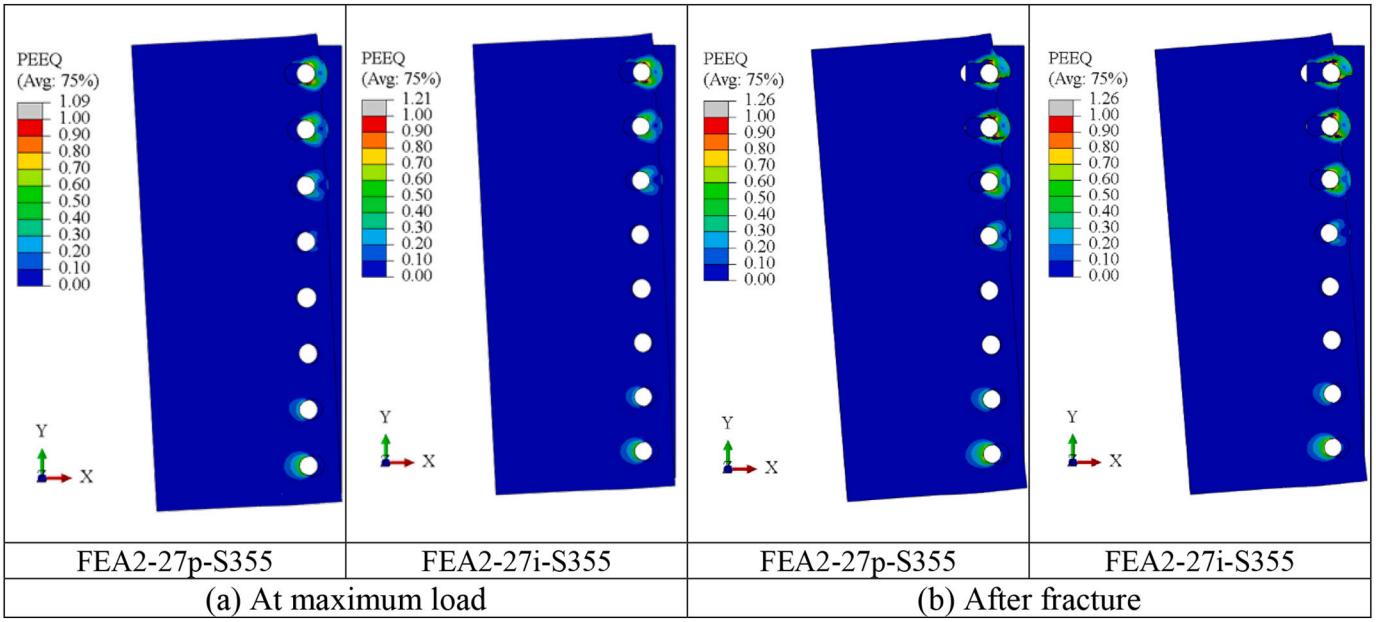

Fig. 20. PEEQ contour plots of FEA2-27-S355 at maximum load and after fracture.

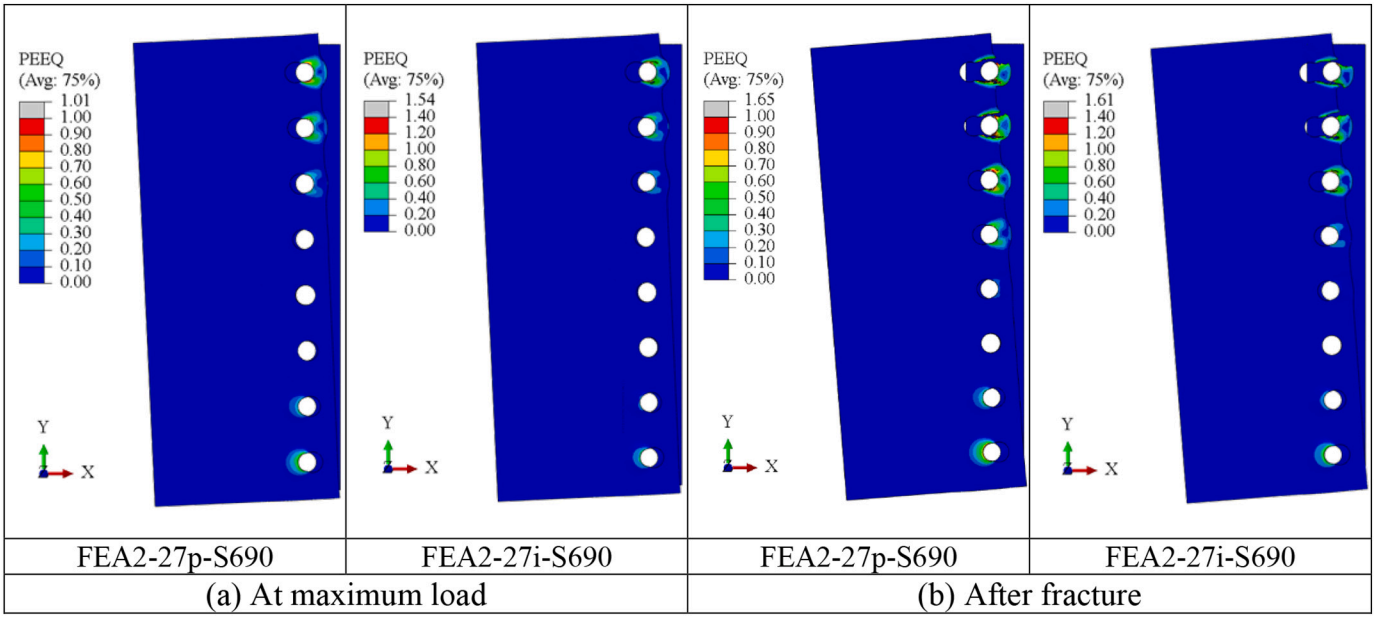

Fig. 21. PEEQ contour plots of FEA2-27-S690 at maximum load and after fracture.

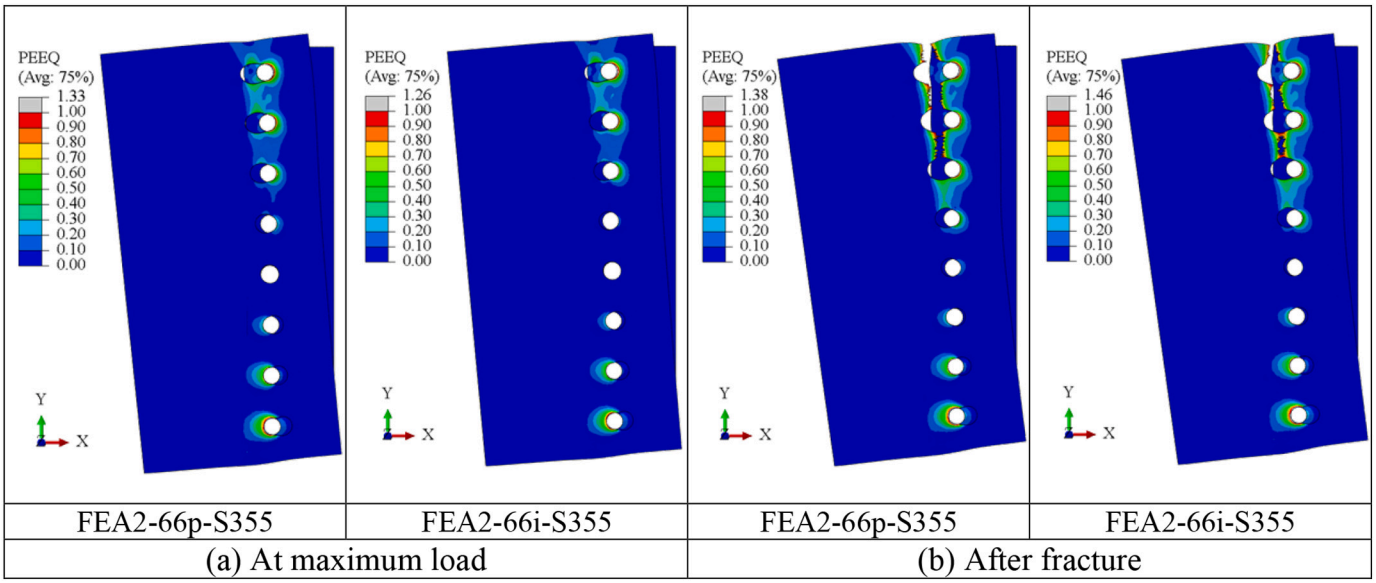

Fig. 22. PEEQ contour plots of FEA2-66-S355 at maximum load and after fracture.

For FEA2-27 connections with short end distance, the bending resistance increases by 33% when moving from linear-elastic to full plastic distribution, where the bearing resistance is the limiting resistance. This agrees with the numerical results where shear-out failure was observed. The predicted forces agree well with the contact forces obtained from the numerical analysis, as shown in Figs. 29 and 30. The FEA2-66 connections with large end distance cannot develop the full bearing resistance due to yielding of the area subjected to tension. Therefore, the resistance is limited by block tearing. It is interesting to observe that all force distributions result in similar bending resistance (see Table 10). Surprisingly, the maximum resistance is given by elastic distribution E for FEA2-66-S355 and elastic-plastic resistance EP2 for FEA2-66-S690. The full plastic distribution of forces does not necessarily give the maximum bending resistance because more deformation capacity is required for full plastic distribution than for any other distribution. This is indirectly accounted for by the block tearing equation. Fig. 30 shows that the bending resistance is well predicted for all connections. Plotted on the *y*-axis in Fig. 30 are the bending moments resulting from the contact forces of the numerical analysis for the connections with imperfect bolt alignment.

The bending resistance was also calculated according to EN 1993-1-8 [1]. The distribution of forces as shown in Fig. 26 was considered, where the maximum resistance of bolts was obtained from the bearing resistance. The bending resistances obtained according to prEN 1993-1-8 and EN 1993-1-8 are shown in Fig. 30. It can be observed that the new approach predicts more accurately the bending resistance for small end distances, while the prediction for large end distances is similar.

The new prEN 1993-1-8 [3] provides an analytical prediction of the moment-rotation behaviour. The rotation is related to the deformation of the bolt hole due to the bearing action. The rotation of the plate can be determined as follows:

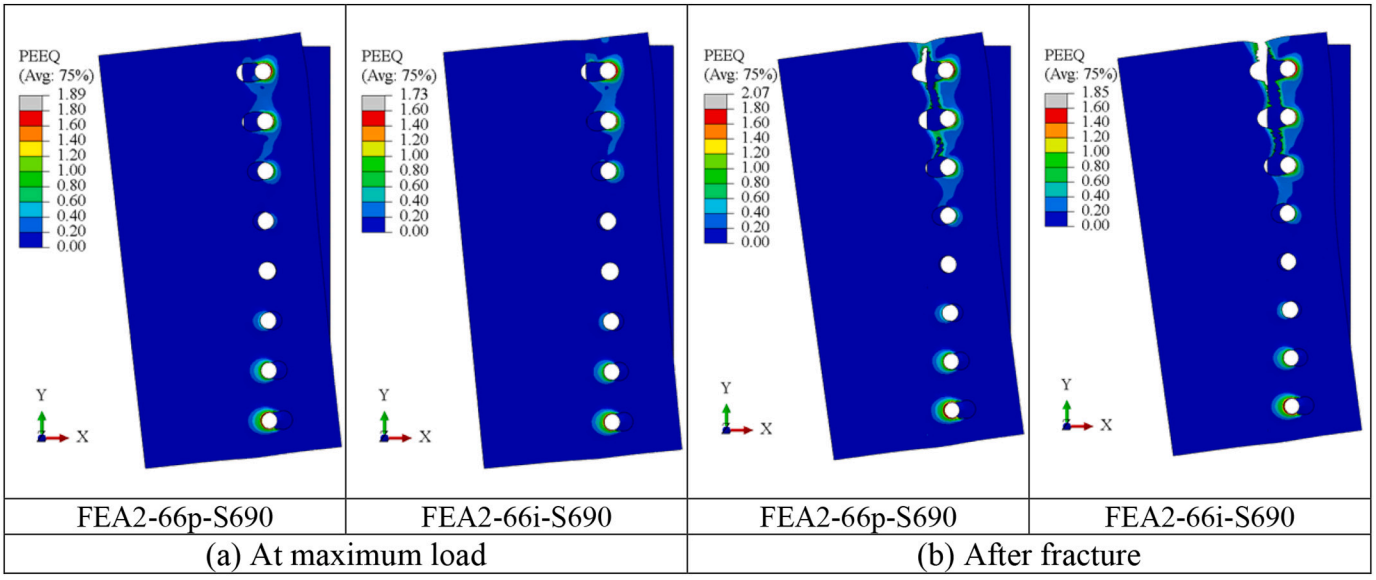

Fig. 23. PEEQ contour plots of FEA2-66-S690 at maximum load and after fracture.

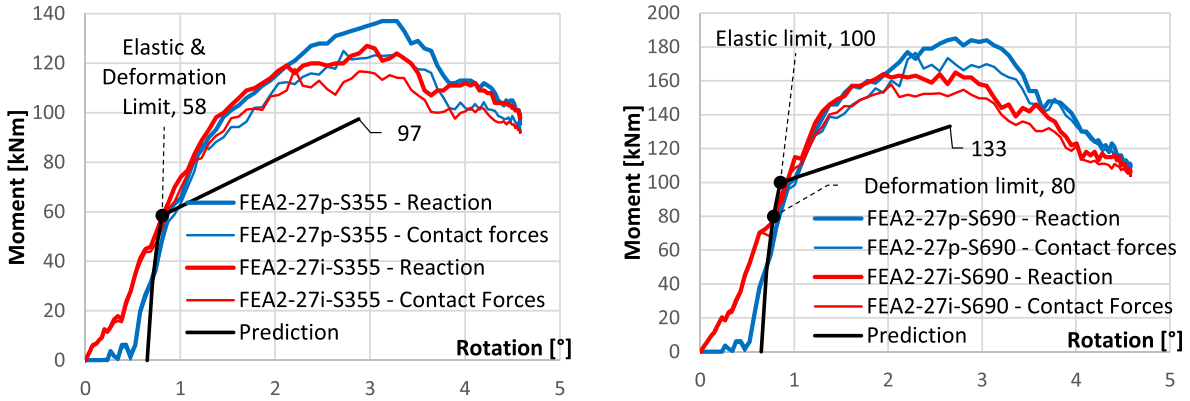

Fig. 24. Moment-rotation curves of FEA2-27.

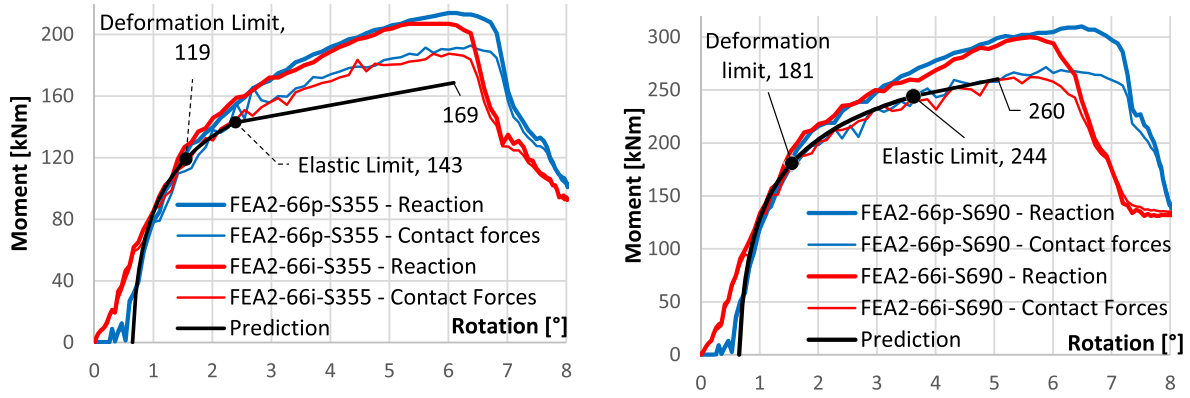

Fig. 25. Moment-rotation curves of FEA2-66.

$$\varphi = arctan\left(\frac{u_1}{r_1}\right) \tag{23}$$

where u_1 is the deformation of the bolt hole 1 and r_1 is the distance from the centre of rotation to the bolt hole 1, as shown in Fig. 26. The initial moment-rotation behaviour is characterized by the embedding of the bolt, where the bolt hole deformation is related to the bearing force, which is obtained as follows:

$$F_1(u_1) = \overline{\sigma}_{b1}\, d\, t f_u \tag{24}$$

where $\overline{\sigma}_{b1}$ is obtained from Eq. (11). The bending resistance in the initial moment-rotation behaviour is obtained assuming the elastic (linear)

Table 8
Summary of FEA results for connections type FEA2.

Connection	Contact force [kN]								Unbalanced force [kN]	Bending moment [kNm]	
	F_1	F_2	F_3	F_4	F_5	F_6	F_7	F_8		from contact forces	from reaction
FEA2-27p-S355	110.4	109.8	107.6	92.7	0.0	−62.0	−168.6	−190.4	−0.6	123.0	137
FEA2-27i-S355	108.4	113.7	110.9	36.3	0.0	−24.5	−157.1	−189.6	−1.9	116.5	127
FEA2-66p-S355	201.7	184.7	162.0	126.9	0.0	−160.7	−227.4	−253.0	34.2	190.2	214
FEA2-66i-S355	206.4	178.2	156.5	103.2	0.0	−140.0	−213.0	−241.4	49.9	182.5	207
FEA2-27p-S690	143.5	152.6	153.8	141.0	0.0	−69.6	−239.9	−268.5	12.8	169.7	185
FEA2-27i-S690	130.3	152.3	155.8	52.1	0.0	0.0	−210.3	−264.5	15.7	152.9	165
FEA2-66p-S690	276.5	259.3	229.5	202.3	0.0	−267.1	−317.3	−339.1	44.1	266.5	310
FEA2-66i-S690	280.9	249.4	249.0	152.9	0.0	−259.7	−300.7	−334.9	36.9	262.2	300

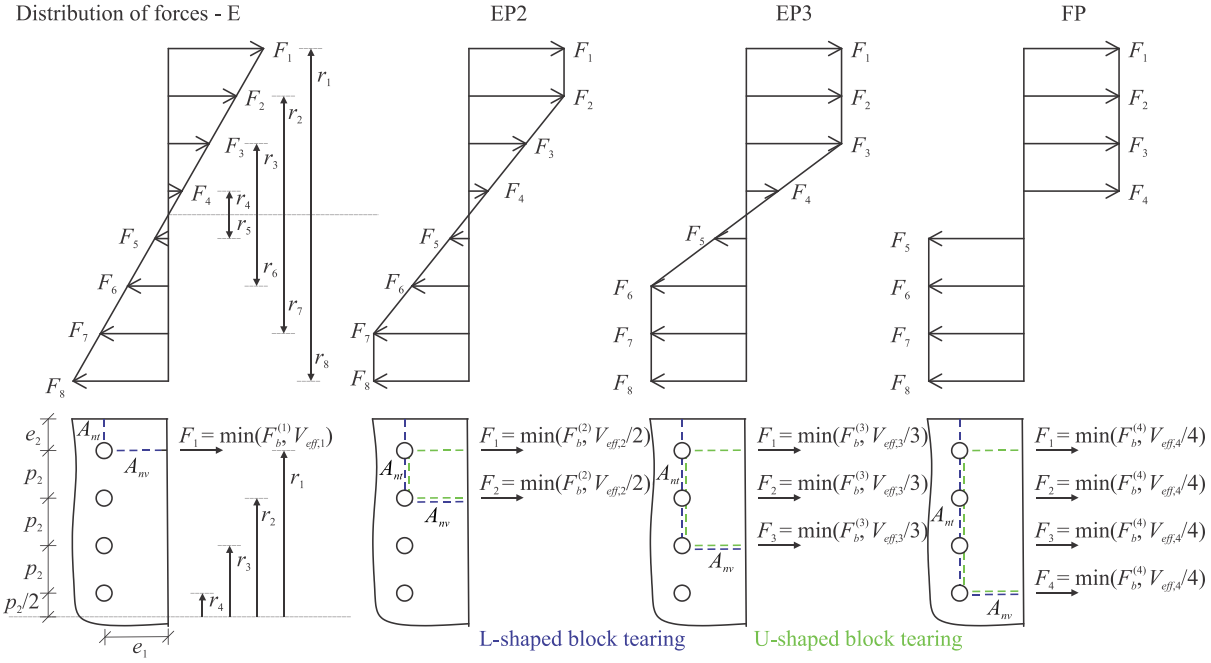

Fig. 26. Assumed distribution of forces between bolts and evaluation of resistances.

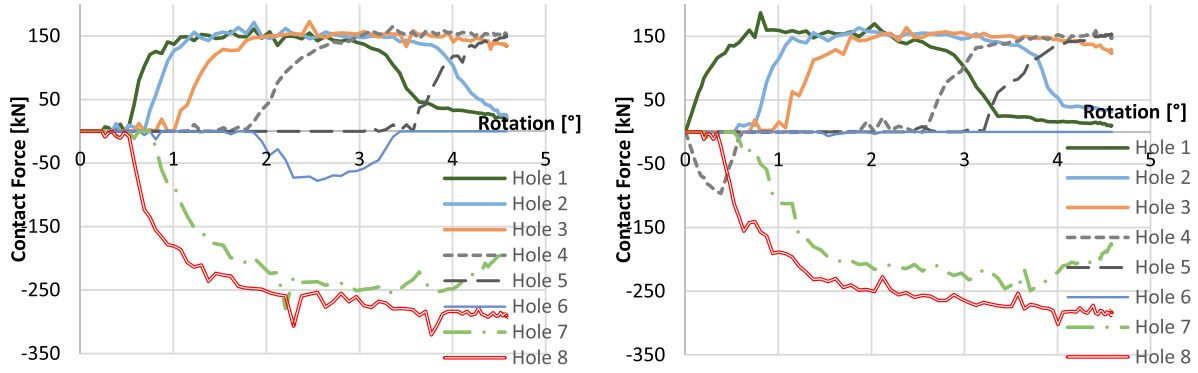

Fig. 27. Contact force – rotation curves for perfect and imperfect bolt hole aligment of S690 connection with short end distance.

distribution of the forces between the bolts:

$$M(u_1) = 2F(u_1)\frac{1}{r_1}\sum_{i=1}^{4} r_i^2 \tag{25}$$

Eq. (11) is valid for grade S355 up to 80% of the maximum bearing resistance and for grade S690 up to the full bearing resistance. The deformation of the bolt hole at the end of validity of Eq. (11) is obtained by inverting the equation considering:

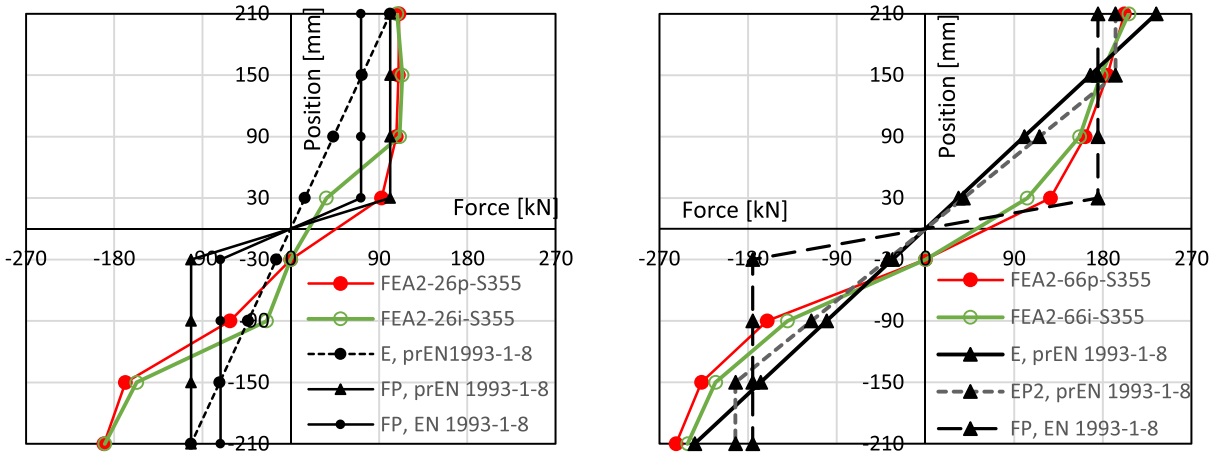

Fig. 28. Distribution of forces between bolts at maximum resistance for FEA2-27-S355 (left) and FEA2-66-S355 (right).

Table 9
Bearing and block tearing resistances according to prEN 1993-1-8.

Unit kN	FEA2-27-S355	FEA2-66-S355	FEA2-27-S690	FEA2-66-S690
F_b	101.5	248.2	138.7	339.1
$V_{eff,1}$	158.2	234.3	240.1	381.5
$V_{eff,2}$	315.3/233.6	391.4/385.8	478.8/354.7	620.2/637.5
$V_{eff,3}$	472.5/345.3	548.6/497.5	717.4/524.2	858.8/807
$V_{eff,4}$	629.7/502.4	705.8/654.6	956.1/762.9	1097.5/1045.7

Note: L-shaped/U-shaped block tearing resistance.

$$\overline{\sigma}_{b1} = \begin{cases} 0.8 k_m \alpha_b & \text{for S355} \\ k_m \alpha_b & \text{for S690} \end{cases} \quad (26)$$

These points are called "Elastic Limit" because the elastic distribution of forces between bolts is assumed and are shown in Figs. 24 and 25. The ultimate bending resistance is determined assuming the fully plastic distribution of the forces between the bolts (see Table 9). The corresponding rotation is obtained as follows:

$$\varphi = arctan\left(\frac{u_{Xd,1}}{r_1}\right) \quad (27)$$

where $u_{Xd,1}$ is the deformation of bolt hole 1 at maximum resistance, which is obtained from Eq. (12). FEA2-27 connections failed in shear out, so $u_{Xd,1}$ corresponds to the hole deformation due to bearing action.

Table 10
Forces on bolts assuming elastic-partial/full plastic distribution, distribution at deformation limit and elastic limit according to prEN 1993-1-8 and bending resistances (units: kN, kNm).

—	FEA2-27-S355					FEA2-66-S355						FEA2-27-S690					FEA2-66-S690				
	DL	E	EP2	EP3	FP	DL	EL	E	EP2	EP3	FP	DL	E	EP2	EP3	FP	DL	E	EP2	EP3	FP
F_1	81	102	102	102	102	165	199	234	193	166	164	111	139	139	139	139	251	339	310	269	261
F_2	58	73	102	102	102	118	142	167	193	166	164	79	99	139	139	139	179	242	310	269	261
F_3	35	44	61	102	102	71	85	100	116	166	164	48	59	83	139	139	108	145	186	269	261
F_4	12	15	20	34	102	24	28	33	39	55	164	16	20	28	46	139	36	48	62	90	261
M	**58**	**73**	**85**	**93**	**97**	**119**	**143**	**169**	**162**	**153**	**157**	**80**	**100**	**117**	**128**	**133**	**181**	**244**	**260**	**247**	**251**

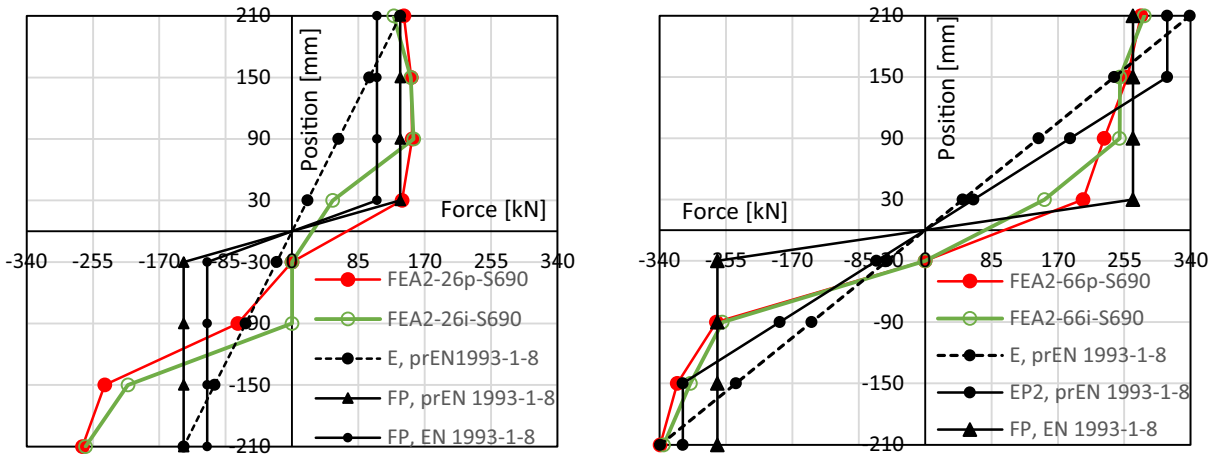

Fig. 29. Distribution of forces between bolts at maximum resistance for FEA2-27-S690 (left) and FEA2-66-S690 (right).

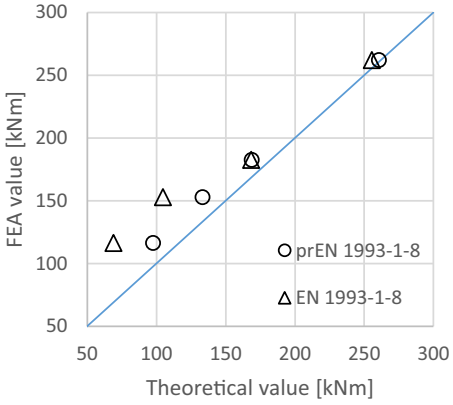

Fig. 30. Comparison of bending resistance according to EN 1993-1-8:2005 and prEN 1993-1-8:2021.

FEA2-66 connections failed in tearing of the area subjected to tension, where high bolt hole deformation due to bearing action can be observed. Therefore, it can be assumed that $u_{\mathrm{Xd},1}$ corresponds to the hole deformation due to the bearing action. A linear relationship is assumed between the elastic limit and the ultimate resistance. The increase of the resistance from the elastic limit to the ultimate resistance is due to redistribution of forces between bolts.

The analytic prediction predicts the moment-rotation behaviour well (see Figs. 24, 25). The predicted behaviour is initially too stiff. This is due to the hole clearance, which does not allow simultaneous contact between the bolt shank and the hole wall. Initially, perfectly aligned bolts float in the clearance hole without resisting rotation. As the plate begins to resist, only the outer bolts begin to bear. The remaining bolts begin to bear as the stiffness increases (at about 30 kNm for the S355 grade and 50 kNm for the S690 grade). After that, the prediction agrees well up to the elastic limit, especially for FEA2-66 with large end distance, where the nonlinear response due to the bearing action can be clearly observed (see Fig. 25).

Moreover, Figs. 24, 25 show the deformation limit. For FEA2-27, the deformation limit coincides with or is just below the elastic limit. For FEA2-66, the deformation limit is the rotation corresponding to the bearing resistance of the outer bolts equal to $2\ d\ t\ f_{\mathrm{u}}$. The hole deformation at $2\ d\ t\ f_{\mathrm{u}}$ is approximately $d_0/6$. This gives the rotation of:

$$\varphi = arctan\left(\frac{22\,\mathrm{mm}/6}{210\ \mathrm{mm}}\right) = 1.00^{\circ} \tag{28}$$

It can be seen that the deformation limit lies in the part of the response curve that can be considered nominally elastic. The distribution of forces between bolts at the elastic limit (EL) and at the deformation limit (DL) is shown in Table 10.

5. Conclusions

The new prEN1993-1-8:2021 for the design of joint in steel structures, which will become available for use in spring of 2023, gives new design formulae for bearing type bolted connections. These formulae, as shown by results, lead to larger design resistances compared to the current EN 1993-1-8:2005. The design formulae generally assume ductile behaviour, so that plastic yielding with strain hardening is indirectly taken into account in the calculation of resistance. Although their reliability was demonstrated using experimental results from the literature, it was not clear whether these formulae were reliable for some specific connections for which there were no experimental results. This was particularly the case for connections where the bearing resistance determines the design. The bearing resistance is dominantly related to the local deformation at the bolt hole. The greater the deformation, the greater the bearing resistance. Since the maximum limit of bearing resistance has been increased, greater local ductility is required to achieve the maximum bearing resistance.

The tests on double lap bolted connections, where 2 bolts were positioned either close to each other or close to the plate edge but far from the plate end edge, showed that the new design formulae underestimate the ultimate resistance by 6% to 14%, while EN 1993-1-8:2005 underestimates the resistances by 38% to 53%. The tests, where 4 bolts were positioned close to each other and far from the plate edges showed that the new design formulae underestimate the ultimate resistance by 15% and 18%, while EN 1993–1-8:2005 underestimates the resistances by 50% and 40%. An interesting test of a connection with two bolts positioned $1.2d_0$ from the longitudinal plate edge, widely spaced and 350 mm from the plate end edge showed an underestimation of resistance by 22% with the new bearing resistance formula and by 57% with the bearing resistance formula according to EN 1993-1-8:2005.

In addition to the experiments on bolted connections, the finite element analysis of very specific bolted connections in S355 and S690 steel was carried out. The FEA is based on the calibrated material models considering the damage initiation and the fracture evolution law with tests on tensile and shear specimens and validated with the experiments on bolted connections. The analysis of bolted connection with widely spaced bolts in 2×2 arrangement, positioned near the plate edge and far from the plate end edge, showed that the new bearing resistance formula overestimates the maximum resistance by 1% for S355 and by 6% for S690. The block tearing formula that determined the design for S355 connection matched the maximum resistance. In this case, the bearing resistance governing the design according to EN 1993-1-8:2005 also significantly underestimated the resistance, by 22% for S355 and 37% for S690.

When the bolt group is loaded by a bending moment, different force distributions between the bolts can be assumed, depending on the available ductility. It was shown that the required ductility can be indirectly controlled by identifying possible failure modes and applying the appropriate design formulae. The method used resulted in a predicted bending moment that underestimated the bending moment obtained by FEA by 1% to 16% when the design formulae according to prEN 1993-1-8:2021 was used. The bending moment obtained according to EN 1993-1-8:2005 was more conservative and underestimated by 3% to 41%.

It can be concluded, based on presented results, that the new design formulae according to pr EN 1993-1-8:2021 lead to reliable prediction of resistances even in very specific cases, satisfying high ductility requirements. The resistances according to pr EN 1993-1-8:2021 can be significantly higher in some tested cases compared to the resistances according to EN 1993-1-8:2005.

Another advantage of the new Eurocode is the new analytical model for predicting the bearing deformation behaviour at the bolt hole. The bearing deformation behaviour shows a non-linear relationship from the application of the bearing force due to the yielding of the material in front of the bolt. For all cases presented, the new bearing deformation model accurately predicted the deformation behaviour of double lap connections and the rotation of the plate with a bolt group loaded by a bending moment. The latter is of great importance since the bending resistance is strongly related to the plate rotation. Based on the bearing deformation model, prEN 1993-1-8:2021 gives the limit of bearing resistance to control the excessive bearing deformation at the bolt hole, which has been proved to be efficient.

Declaration of Competing Interest

The authors declare that they have no known competing financial interests or personal relationships that could have appeared to influence the work reported in this paper.

Acknowledgements

The first author acknowledges the financial support from the Slovenian Research Agency (research core funding No. P2-0158).

References

[1] CEN, Eurocode 3: Design of Steel Structures - Part 1–8: Design of Joints, EN 1993-1-8, Belgium, 2005.
[2] CEN, Eurocode 3: Design of Steel Structures - Part 1–1: General Rules and Rules for Buildings, EN 1993-1-1, 2005.
[3] CEN, Eurocode 3: Design of Steel Structures - Part 1–8: Design of Joints, PrEN 1993-1-8, 2021, p. 197.
[4] P. Može, Statistical evaluation of bearing resistance and related strength functions for bolted connections, J. Constr. Steel Res. 171 (2020) 106–128, https://doi.org/10.1016/j.jcsr.2020.106128.
[5] AISC, Specifications for Structural Steel Buildings, ANSI/AISC 360-16, 2016.
[6] R.M. Richard, M.K.Z. Elsalti, Moment-rotation curves for partially restrained connections, in: Users Man. Progr. Dev. Univ. Arizona, 1991.
[7] C.O. Rex, W.S. Easterling, Behavior and modeling of a bolt bearing on a single plate, J. Struct. Eng. 129 (2003) 792–800, https://doi.org/10.1061/(Asce)0733-9445(2003)129:6(792).
[8] P. Može, Deformation behavior of bolted bearing-type connections, in: 9th Int. Work. Connect. Steel Struct., Coimbra, Portugal, 2022.
[9] M. Veljkovic, M. Couchaux, A. Giraõ Coelho, P. Može, A. Stratan, F. Wald, CEN/TC 250/SC 3/WG 8 N 118: Mandate M515 – Project SC3.T2 - Background Documents for the Revision of Eurocode 3 Part 1–8, 2018.
[10] P. Može, Deformation capacity, stiffness and bearing strength at bolt holes, in: 8th Int. Work. Connect. Steel Struct, AISC, Boston, USA, 2016.
[11] P. Može, D. Beg, Investigation of high strength steel connections with several bolts in double shear, J. Constr. Steel Res. 67 (2011) 333–347.
[12] CEN, Eurocode 3 — Design of Steel Structures — Part 1-1: General Rules and Rules for Buildings, PrEN1993-1-1, 2020.
[13] M. Feldmann, S. Schaffrath, Assessing the net section resistance and ductility requirements of EN 1993-1-1 and EN 1993-1-12, Steel Constr. 10 (2017) 354–364, https://doi.org/10.1002/stco.201710036.
[14] Abaqus Analysis User's Guide, Version 2020. https://www.3ds.com/products-services/simulia/products/abaqus/, 2020.
[15] H.C. Ho, K.F. Chung, X. Liu, M. Xiao, D.A. Nethercot, Modelling tensile tests on high strength S690 steel materials undergoing large deformations, Eng. Struct. 192 (2019), https://doi.org/10.1016/j.engstruct.2019.04.057.
[16] Y. Ling, Uniaxial true stress-strain after necking, AMP J. Technol. 5 (2004).
[17] F. Yang, M. Veljkovic, Y. Liu, Ductile damage model calibration for high-strength structural steels, Constr. Build. Mater. 263 (2020) 120632, https://doi.org/10.1016/j.conbuildmat.2020.120632.
[18] F. Yang, M. Veljkovic, Damage model calibration for S275 and S690 steels, Ce/Papers 3 (2019) 262–271, https://doi.org/10.1002/cepa.1201.
[19] Y. Bao, T. Wierzbicki, On fracture locus in the equivalent strain and stress triaxiality space, Int. J. Mech. Sci. 46 (2004) 81–98, https://doi.org/10.1016/j.ijmecsci.2004.02.006.
[20] F. Yang, Y. Liu, H. Xin, M. Veljkovic, Fracture simulation of a demountable steel-concrete bolted connector in push-out tests, Eng. Struct. 239 (2021) 112305, https://doi.org/10.1016/J.ENGSTRUCT.2021.112305.